Implications of the ongoing rock uplift in NW Himalayan interiors

Saptarshi Dey[1], Rasmus C. Thiede[2], Arindam Biswas[3], Naveen Chauhan[4], Pritha Chakravarti[1], and Vikrant Jain[1]

[1]*Earth Science Discipline, IIT Gandhinagar, Gandhinagar-382355, India.*

[2]*Institute of Geosciences, Christian Albrechts University of Kiel, Kiel-24118, Germany.*

[3] *Department of Applied Geology, IIT-ISM Dhanbad, Jharkhand-826004, India.*

[4] *Atomic Molecular and Optical Physics Division, Physical Research Laboratory, Ahmedabad.*

Corresponding author

Saptarshi Dey

saptarshi.dey@iitgn.ac.in

Abstract

The Lesser Himalaya exposed in the Kishtwar Window (KW) of the Kashmir Himalaya exhibits rapid rock uplift and exhumation (~3 mm/yr) at least since the Late Miocene. However, it has remained unclear if it is still actively-deforming. Here, we combine new field, morphometric and structural analyses with dating of geomorphic markers to discuss the spatial pattern of deformation across the window. We found two steep stream segments, one at the core and the other along the western margin of the KW, which strongly suggest ongoing differential uplift and may possibly be linked either to crustal ramps on the MHT or active surface-breaking faults. High bedrock incision rates (> 3 mm/yr) on Holocene/Pleistocene timescales are deduced from dated strath terraces along the deeply-incised Chenab River valley. In contrast, farther

downstream on the hanging wall of the MCT, fluvial bedrock incision rates are lower (< 0.8 mm/yr) and are in the range of long-term exhumation rates. Bedrock incision rates largely correlate with previously-published thermochronologic data. In summary, our study highlights a structural and tectonic control on landscape evolution over millennial timescales in the Himalaya.

Keywords

Steepness index; knickzone, rock strength; bedrock incision; Main Himalayan Thrust.

1. Introduction

Protracted convergence between the Indian and the Eurasian plate resulted into the growth and evolution of the Himalayan orogen and temporal in-sequence formation of the Southern Tibetan Detachment System (STDS), the Main Central Thrust (MCT), the Main Boundary Thrust (MBT) and the Himalayan Frontal Thrust (HFT) towards the south (e.g., Yin and Harrison, 2000; DiPietro and Pogue, 2004) (Supplementary Fig.B1). The HFT defines the southern termination of the Himalayan orogenic wedge and separates the orogen from the undeformed foreland basin known as the Indo-Gangetic Plains. Seismic reflection profiles reveal that all these fault-zones emerge from a low-angle basal decollement, the Main Himalayan Thrust (MHT) forming the base of the Himalayan orogenic wedge (e.g., Ni and Barazangi, 1984; Nabelek et al., 2009; Avouac et al., 2016), established in the late Miocene (Vannay et al., 2004). Existence of the MHT has further been elaborated in Himalayan cross-sections (e.g., Powers et al., 1998; Decelles et al., 2001; Webb et al., 2011; Gavillot et al., 2018).

Lave and Avouac (2000) studied the late Pleistocene-Holocene shortening history of the Central Nepal Himalaya where they showed the Holocene shortening is accommodated only across the HFT. However, a large body of literature in the eastern, central and western Himalaya favored that the majority of the late Pleistocene-Holocene shortening is rather partitioned throughout the Sub-Himalayan domain (morphotectonic segment in between the MBT and the MFT) and not solely accommodated by the HFT (e.g., Wesnousky et al., 1999; Burgess et al., 2012; Thakur et al., 2014; Mukherjee, 2015; Vassalo et al., 2015; Dey et al., 2016; Dey et al., 2018). The statement above implies that the northerly thrusts, i.e., the MBT and the brittle faults exposed in the vicinity of the southern margin of the Higher Himalaya, are considered inactive over millennial timescales. However, in recent years, several studies which focused on the low-temperature thermochronologic data and thermal modeling of the interiors of the NW Himalaya have raised questions on the statement above. The recent studies suggested that 1-3 mm/yr out of the total Quaternary shortening has been accommodated in the north of the MBT as out-of-sequence deformation (Thiede et al., 2004; Deeken et al., 2011; Thiede et al., 2017) or in form of growth of the Lesser Himalayan Duplex (Gavillot et al., 2018) (Supplementary Fig. B2). For faults within the hinterland of the Central Himalaya, the out-of-sequence deformation has been explained by two end-member models. One of them favored the reactivation of the MCT (Wobus et al., 2003), while the other tried to explain all changes along the southern margin of the Higher Himalaya driven by enhanced rock uplift over a major ramp on the MHT (Bollinger et al., 2006; Herman et al., 2010; Robert et al., 2009). Landscape evolution models, structural analysis and thermochronologic data from the interior of the Himalaya favor that the Lesser Himalaya has formed a duplex at the base of the southern Himalayan front by sustained internal deformation since late Miocene (Decelles et al., 2001; Mitra et al., 2010; Robinson and Martin, 2014; Gavillot

et al., 2016). The growth of the duplex resulted in the uplift of the Higher Himalaya forming the major orographic barrier of the orogen. The Kishtwar Window (KW) in the NW Himalaya represents the northwestern termination of the Lesser Himalayan Duplex (LHD). While most of the published cross-sections of the Himalayan orogen today recognize the duplex structures within the Lesser Himalaya (Webb et al., 2011; Mitra et al., 2010; DeCelles et al., 2001; Gavillot et al., 2018), little or no data are available on how the deformation is spatially as well as temporally distributed and most importantly, whether a duplex is active over millennial timescales.

The low-temperature thermochronology study by Kumar et al. (1995) portrayed the first orogen-perpendicular sampling traverse extending from the Kishtwar tectonic Window over the Zanskar Range. More recent studies link the evolution of the KW to the growth of the Lesser Himalayan Duplex structure (Gavillot et al., 2018), surrounded by the Miocene MCT shear zone along the base of the High Himalayan Crystalline, locally named as the Kishtwar Thrust (KT) (Ul Haq et al., 2019). Thermochronological constraints suggest higher rates of exhumation within the window (3.2-3.6 mm/yr) with respect to the surroundings (~0.2 mm/yr) (Gavillot et al., 2018), corroborating similar thermochronology-based findings from the of the Kullu-Rampur window along the Beas (Stübner et al., 2018) and Sutlej valley (Jain et al., 2000; Vannay et al., 2004; Thiede et al., 2004) over Quaternary timescales. No evidence exists to distinguish whether the hinterland of the Kashmir Himalaya is tectonically-active over intermediate timescales. Therefore, to understand the 10^3-10^4-year timescale neotectonic evolution, we combined geological field evidence, chronologically-constrained geomorphic markers and morphometric analysis of the KW. The detailed structural information of the window and its surroundings, previously-published thermochron data, accessibility, well-preserved sediment archives, and

recognizable geomorphic markers across the Kishtwar Window makes it an attractive location for our study.

In this study, we use the KW to focus on the following long-standing questions on Himalayan neotectonic evolution, which are-

1. Is there any ongoing neotectonic deformation in the interiors of the Kashmir Himalaya?

2. Can we determine sub-surface structural variations and existence of surface-breaking faults by analyzing terrain morphology?

3. Can we obtain new constraints on deformation over geomorphic timescales? Do millennial-scale fluvial incision rates support long-term exhumation rates?

To address these questions, we adopted a combination of methods including morphometric analysis using high-resolution digital elevation models, field observations on rock type, structural variations as well as rock strength data, and analysis of satellite images to assess the spatial distribution of the late Quaternary deformation of the KW and surroundings (fig. 1). We aimed to evaluate the role of active tectonics and geometric variations in the basal decollement in shaping the topography (Fig.1). We used basinwide steepness indices and specific stream power as a proxy of fluvial incision. And, lastly but most importantly, we calculated the fluvial bedrock incision rates by using depositional ages of aggraded sediments along Chenab River. In this study, we show that the regional distribution of topographic growth is concentrated in the core of the window and along the western margin of the window. Our new estimates of bedrock incision rate agree with Quaternary exhumation rates from the KW, which could mean consistent active growth of the Kishtwar Window over million-year to millennial timescales.

Although the observed topographic and morphometric pattern indicate a structural/tectonic control on topographic evolution, with the available data we are not able to resolve whether it is caused by passive translation on the MHT or by active surface-breaking faulting within the duplex.

2. Geological background

Regionally balanced cross-sections (DiPietro and Pogue, 2004; Searle et al., 2007; Gavillot et al., 2018) suggest that the Himalayan wedge is bounded at the base by a décollement, named the MHT. All regionally-extensive surface-breaking thrust systems are thought to be rooted to the MHT. The orogenic growth of the Himalaya resulted into an overall in-sequence development of the orogen-scale fault systems which broadly define the morphotectonic sectors of the orogen (fig. 1b). Notable among those sectors, the Higher Himalaya is bordered by the MCT in the south and is comprised of high-grade metasediments, Higher Himalayan Crystalline Sequence (HHCS) and Ordovician granite intrusives (Fuchs, 1981; Steck, 2003; DiPietro and Pogue, 2004; Gavillot et al., 2018). The low-grade metasediments (quartzites, phyllites, schists, slates) of the Proterozoic Lesser Himalayan sequence are exposed between the MCT in the north and MBT in the south. The Lesser Himalayan domain is narrow (4-15 km) in the NW Himalaya except where it is exposed in the form of tectonic windows (Kishtwar window, Kullu-Rampur window etc.) in the western Himalaya (Steck, 2003). The Sub-Himalayan fold-and-thrust belt lying to the south of the MBT is tectonically the most active sector since the late Quaternary (Gavillot, 2014; Vassallo et al., 2015; Gavillot et al., 2018).

Near the southwest corner of our study area, Proterozoic low-grade Lesser Himalayan metasediments are thrust over the Tertiary Sub-Himalayan sediments along the MBT (Wadia, 1934; Thakur, 1992). Near the Chenab region in the Kashmir Himalaya, apatite U-Th/He ages suggest that cooling and exhumation related to faulting along the MBT thrust sheet initiated before ~5 ± 3 Myr (Gavillot et al., 2018). Geomorphic data obtained across the MBT in Kashmir Himalaya suggest that MBT has not been reactivated for the last 14-17 kyr (Vassallo et al., 2015). In the Kashmir Himalaya, the Lesser Himalayan sequence (LHS) exposed between the MBT and the MCT is characterized by a < 10 km-wide zone of sheared schists, slates, quartzites, phyllites and Proterozoic intrusive granite bodies (Bhatia and Bhatia, 1973; Thakur, 1992; Steck, 2003). The LHS is bounded by the MCT shear zone in the hanging wall. The MCT hanging wall forms highly deformed nappe exposing lower and higher Haimantas, which are related to the Higher Himalayan Crystalline Sequence (HHCS) (Bhatia and Bhatia, 1973; Thakur, 1992; Yin and Harrison, 2000; Searle et al., 2007; Gavillot et al., 2018). Nearly 40 km NE of the frontal MCT shear zone, MCT fault zone is re-exposed as a klippe in the vicinity of KW and is called the Kishtwar Thrust (KT) (Ul Haq et al., 2019) (fig. 1). Within the KW, Lesser Himalayan quartzites, low-grade mica schists and phyllites along with the granite intrusives are exposed (Fuchs, 1975; Steck, 2003; DiPietro and Pogue, 2004; Yin, 2006; Gavillot et al., 2018).

2.1. Structural architecture of the Kishtwar Window

The sub-surface structural formation beneath the KW is not well-constrained. A recent study by Gavillot et al., (2018) proposes that the KW exposes a stack of LHS nappes in form of the commonly-known Lesser Himalayan Duplex (LH duplex), characteristic of the central Himalaya (Decelles et al., 2001). They also propose the existence of two mid-crustal ramps beneath the KW, viz., MCR-1 and MCR-2 (fig. 1b). Based on thermochronological constraints

156 from Kumar et al., (1995), Gavillot et al. (2018) proposed that the core of the window has been
157 exhumed at rates of 3.2-3.6 mm/yr during the Quaternary, at a higher rate when compared to the
158 surroundings (~0.2-0.4 mm/yr). However, earlier studies by Fuchs (1975) and Frank et al.,
159 (1995) provide different interpretations of the formation of the KW. Fuchs (1975) proposed the
160 existence of two nappes- a. the Chail Nappe and b. the Lower Crystalline Nappe. The Lower
161 Crystalline nappe is partially or completely included in the MCT (KT) shear zone and the Chail
162 nappe encompasses the core of the window (Stephenson et al., 2000). According to these studies,
163 the Chail nappe has been internally deformed by crustal buckling, tight isoclinal folding causing
164 repetition and thickening of the LH crust.

165 The Higher Himalayan sequence dips steeply away from the duplex (~65° towards west)
166 (fig. 1, 2a). The frontal horses of the LH duplex expose internally-folded greenschist facies
167 rocks. Although at the western margin of the duplex, the quartzites stand sub-vertically (fig. 2c),
168 the general dip amount reduces as we move from west to east for the next ~10-15 km up to the
169 core of the KW. Near the core of the KW, we observed highly-deformed (folded and multiply-
170 fractured) quartzite at the core of the KW (fig. 2d, 2e). We also observed deformed quartz veins
171 of at least two generations, as well as macroscopic white mica. Here, the Chenab River is also
172 very steep and narrow; the rock units are also steeply-dipping towards the east (~55-65°) and are
173 nearly isoclinal and strongly deformed at places (fig. 2f). Towards the eastern edge of the
174 window, however, the quartzites dip much gently towards the east (~20-30°) (fig. 1b), and much
175 lesser folding and faulting have been recognized in the field (fig. 2g).

176 **2.2. Valley morphology**

177 The broad, ‘U-shaped’ valley profile near the town of Padder at the eastern margin of the
178 KW is in contrast with the interior of the window (Fig.3a). At the core of the KW, the Chenab

River maintains a narrow channel width and a steep gradient (fig. 3b). The E-W traverse of the Chenab River through the KW is devoid of any significant sediment storage. However, along the N-S traverse parallel to the western margin of the KW, beneath the Kishtwar surface, ~150-170m thick sedimentary deposits are transiently-stored over the steeply-dipping Higher Himalayan bedrock (fig. 3c). The height of the Kishtwar surface from the Chenab River is ~450m, which means ~280m of bedrock incision by the river since the formation of the Kishtwar surface. Along the N-S traverse of the River, epigenetic gorges are formed as a result of the damming of paleo-channel by the hillslope debris flow, followed by the establishment of a newer channel path (Ouimet et al., 2008; Kothyari and Juyal, 2013). One example of such epigenetic gorge formation near the town of Drabshalla is shown in fig. 3d. Downstream from the town of Drabshalla, the river maintains narrow channel width (< 25 m) and flows through a gorge having sub-vertical valley-walls (fig. 3e). The tributaries originating from the Higher Himalayan domain form one major knickpoint close to the confluence with the trunk stream (fig. 3f). We have identified at least three strath surface levels above the present-day river channel, viz., T1 (280±5 m), T2 (170-175 m) and T3 (~120±5 m), respectively (fig. 3g). The first study on sediment aggradation in the middle Chenab valley (transect from Kishtwar to Doda town) was published by Norin (1926). He argued the sediment aggradation in and around the Kishtwar town is largely contributed by fluvioglacial sediments and the U-shaped valley morphology is a marker of past glacial occupancy. In general, we agree with the findings of Norin (1926) and Ul Haq et al., (2019) as we observe ~100m thick late Pleistocene fluvioglacial sediment cover unconformably overlying the Higher Himalayan bedrock, most likely to be paleo-strath surface (fig. 4b). At the same time, we do not agree with the interpretation of surface-breaking faults near Kishtwar town by Ul Haq et al. (2019). We inspected the proposed fault locations in detail and did not observe

any evidence of large-scale fault movement, including offset, broken and rotated clasts, fault gouges etc. on the proposed fault planes. There is evidence of only one deformed sand layer which shows tilting and offset (<1 m). Therefore, we conclude that we found no strong evidence of any large-scale surface-breaking faults. The fluvioglacial sediments included alternate layers of pebble conglomerate and coarse-medium sand (fig. 4c). The pebbles are moderately rounded and polished suggesting significant fluvial transport. Our field observations suggest that the fluvioglacial sediments have been succeeded by a significant volume of hillslope debris flow and paleo-landslide deposit (fig. 4c). The thickness of the debris-flow deposits is variable. The hillslope debris units and landslide deposits contain mostly massive, highly-angular, poorly-sorted quartzite clasts from the steep western margin of the KW. The hillslope debris units also contain a few fine-grain sediment layers trapped in between two coarse-grained debris layers (fig. 4e). The town of Kishtwar is situated on this debris flow deposit.

3. Methods of morphometric analysis and field data collection

3.1. Morphometry

For conducting the morphometric analysis, we have used 12.5m ALOS-PALSAR DEM data (high resolution terrain-corrected) (fig. 5a). This DEM data has lesser issues with artifacts and noises than 30m SRTM data, which fails to capture the drainage network properly in areas populated by narrow channel gorges. Topographic relief has been calculated using a 4km moving window (fig. 5b) and the rainfall distribution pattern has been adapted from 12-year averaged annual rainfall data (TRMM data: Bookhagen and Burbank, 2006) (fig. 5c).

3.1.1. Drainage network extraction

The drainage network and the longitudinal stream profiles were extracted using the Topographic Analysis Kit toolbox (Forte and Whipple, 2019). An equivalent of 10-pixel smoothing of the raw DEM data has been applied to remove noises from the DEM. The longitudinal stream profile of the Chenab trunk stream was processed with the Topotoolbox 'Knickpointfinder' tool (Schwanghart and Scherler, 2014). Several jumps/ kinks in the longitudinal profile are seen and those are marked as knickpoints (fig. 6). A 30m tolerance threshold was applied to extract only the major knickpoints.

3.1.2. Basinwide normalized steepness indices

Global observations across a broad spectrum of tectonic and climatic regimes have revealed a power-law scaling between the local river gradient and upstream contributing area:

$$S = k_s . A^{-\theta} \qquad \text{(Eq. 1)}$$

where S is the stream gradient (m/m), k_s is the steepness index ($m^{2\theta}$), A is the upstream drainage area (m^2), and θ is the concavity index (Flint, 1974; Whipple and Tucker, 1999). Normalized steepness-index values (k_{sn}) are steepness indices calculated using a reference concavity value (θ_{ref}), which is useful to compare steepness-indices of different river systems (Wobus et al., 2006). We extracted the k_{sn} values in the study area using the ArcGIS and MATLAB-supported Topographic Analysis Toolkit (Forte and Whipple, 2019) following the procedure of Wobus et al. (2006). We performed an automated k_{sn} extraction using a critical area of 10^6 m^2 for assigning the channel head, a smoothing window of 500 m, a θ_{ref} of 0.45, and an auto-k_{sn} window of 250 m for calculating k_{sn} values. The slope-breaks, known as the knickpoints (sometimes referred to as knickzones if it is manifested by a series of rapids instead of a single sharp break in profile), were allocated by comparing the change of slope along the distance-elevation plot (fig. 6, 7a). Threshold 'dz' value (projected stream offset across a knickpoint) for

248 this study is 30m. Basinwide mean k_{sn} values are plotted using a 1000 km^2 threshold catchment
249 area (fig. 5d).

250 Identification of the knickpoints/ knickzones and their relationship with the rock-types as
251 well as with existing structures are necessary to understand the causal mechanism of the
252 respective knickpoints/ knickzones. Knickpoints/(zones) can be generated by lithological,
253 tectonic and structural control. Lithological knickpoints are stationary and anchored at the
254 transition from the soft-to-hard substrate. The tectonic knickpoints originate at the active tectonic
255 boundary and migrate upstream with time. Structural variations, such as thrust fault ramp-flat
256 geometry, may cause a quasistatic knickpoint at the transition of the flat-to-ramp of the fault. In
257 such cases, the ramp segment is characterized by higher steepness than the flat segment and at
258 times the ramp may be characterized by a sequence of rapids, forming a wide knickzone, instead
259 of a single knickpoint.

260 ***3.1.3. Channel Width***

261 Channel width is a parameter of assessment of lateral erosion/incision through bedrocks
262 of equivalent strength (Turowski, 2009). The channel width of the Chenab trunk stream from just
263 downstream of the MBT up to the eastern margin of the KW was derived by manual selection
264 and digitization of the channel banks using the Google Earth Digital Globe imagery
265 (http://www.digitalglobe.com/) of minimum 3.2 m spatial resolution. We used the shortest
266 distance between the two banks as the channel width. We rejected areas having unparallel
267 channel-banks as that would bias the result. We used a 50 m step between two consecutive points
268 for channel width determination. Twenty point-averaged channel width data along with elevation
269 of the riverbed is shown in fig. 7b.

270 ***3.1.4. Specific stream power (SSP) calculation***

Specific stream power has often been used as a proxy of fluvial incision or differential uplift along the channel (Royden and Perron, 2013; Whipple and Tucker, 1999). Areas of higher uplift/incision are characterized by transient increase in the specific stream power. Channel slope and channel width data were used to analyse the corresponding changes in the specific stream power (SSP) from upstream of the gorge area to the gorge reaches (Bagnold, 1966). The SSP (ω) was estimated using the following equation –

$$\omega = \gamma . Q . s / w \qquad \text{(Eq. 2)}$$

Where, γ - unit weight of water, Q – water discharge, s – energy slope considered equivalent to the channel slope; w – channel width. SSP data from selected stretches are shown in Table 1. Channel width has been adapted from method described in section 3.1.3. We assumed a uniform discharge throughout the study area, as the TRMM data show insignificant variations in mean annual rainfall (Bookhagen and Burbank, 2006) (fig. 5c, 5e). We also assume a runoff ratio of 1 as we lack any independent measure or supportive data of runoff vs. water percolation through the bedrock and sediment archive.

3.2. Field data collection

3.2.1. Structural data

We measured the strike and dip of the foliations and bedding planes of the Lesser and Higher Himalayan rocks using the Freiberg clinometer compass. At least five measurements are taken at every location and the average of them has been reported in fig. 8a. Field photos in the fig. 2 support observed variations in the structural styles.

3.2.2. Rock strength data

Recording rock strength data in the field is important to understand the role of variable rock-type and rock-strength in changes in morphology. It provides us important insights on the genesis of knickpoints whether they are lithologically-controlled or not. It also helps to understand the variations in channel steepness across rocks of similar lithological strength. We systematically measured the rock strength of the main geologic units using a hand-held rebound hammer. Repeated measurements (8-10 measurements at each of the 75 locations throughout the study area) were conducted to measure the variability of rock-strength within the main lithologic units (fig. 7e). All the measurements were taken perpendicular to the bedding/ foliation plane, and no measurements are from wet surfaces or surfaces showing fractures. Each reading was taken at least 0.5m apart from the previous one. To our benefit, most of the road-cut sections had bedrock-exposures. Except restricted locations, e.g., dam-sites and military bases and outposts, we were able to cover all of the study area. However, data taken from Higher Himalayan intrusives close to the western margin of the KT are positively-biased as it represents readings only from the leucosomatic layers. Our data from individual sites are smaller in number than what is preferred for checking the statistical robustness of Schmidt hammer data (Niedzielski et al., 2009). Therefore, we combined the data from all sites representing similar lithology and portrayed the mean ±standard deviation for each rock type. Field data on rock strength measurement have been provided in Supplementary Table C1.

3.3. Luminescence dating of transiently-stored sediments in and around Kishtwar

Luminescence dating of Quaternary sediments is a globally accepted method for constraining the timing of deposition of sediments across different depositional environments, viz., aeolian (Juyal et al., 2010), fluvial (Olley et al., 1998; Cunningham and Wallinga, 2012) and glacial origin (Owen et al., 2002; Pant et al., 2006). In this study, we used luminescence

316 dating to constrain depositional ages of several fluvioglacial and fluvial sand layers exposed near
317 the western margin of the KW and further downstream. Although there exists a few persistent
318 problems in luminescence dating of the Himalayan sediments (including poor sensitivity of
319 quartz and numerous cases of heterogeneous bleaching of the luminescence signal), studies over
320 the past couple of decades have also provided a good control on Himalayan sedimentary
321 chronology by using luminescence dating with quartz (Optically stimulated luminescence, OSL)
322 and feldspar (Infra-red stimulated luminescence, IRSL).

323 Samples K-07, K-08 and K-09 were collected from the medium-coarse sand beds of
324 fluvioglacial origin and have been dated with IRSL technique (Preusser, 2003). Standard IR-
325 protocol was used because the OSL signal was saturated and postIR-IR was showing instances of
326 heterogeneous bleaching. Samples K-02 and K-11 were taken from the fine sand-silt layers lying
327 above the debris-flow deposits and have been treated for OSL dating using double-SAR (single
328 aliquot regenerative) protocol (Roberts, 2007). Double-SAR protocol was used to surpass the
329 luminescence signal from tiny feldspar inclusions within individual quartz grains. Samples K-16
330 and K-17 taken above the T3 strath level, as well as the sample K-18, taken from above the T1
331 strath level, were treated/ measured following the OSL double-SAR protocol. Samples K-01 and
332 K-06 taken above the bedrock strath near the town of Doda were also measured following OSL
333 double-SAR protocol. The aliquots were considered for equivalent dose (ED) estimation only if:
334 (i) recycling ratio was within 1±0.1, (ii) ED error was less than 20%, (iii) test dose error was less
335 than 10%, and (iv) recuperation was below 5% of the natural. Fading corrections of the IRSL
336 samples K-07 and K-09 were done using conventional methods (Huntley and Lamothe, 2001).
337 For samples showing over-dispersion (OD) ≤20%, central age model (CAM) was used for
338 estimation of equivalent dose (De) (Bailey and Arnold, 2006) instead of RMM-based De

estimation as prescribed by Chauhan and Singhvi, (2011), useful for samples having higher over dispersion (Table 2). For samples K-16 and K-17 having high OD value, the minimum age model (MAM) was used. Details of sample preparation are provided in supplement.

The dose rate was estimated using online software DRAC (Durcan et al., 2015) from the data of Uranium (U), Thorium (Th) and Potassium (K) measured using ICP-MS and XRF (Table 2) in IISER Kolkata. The estimation of moisture content was done by using the fractional difference of saturated vs. unsaturated sample weight (Table 2).

4. Results

4.1. Field observations and measurements

The Chenab River has deeply incised the KW (fig. 3b and 3e). The LHS rock units exposed within the KW are mainly composed of fine-grain quartzites and phyllites with occasional schists in between (Steck, 2003; Gavillot et al. 2018). The Lesser Himalaya has been suggested to be an asymmetric antiformal stack with a steeper western flank (dip: 70°/west) (fig. 2c). The KW is surrounded by rock units related to the Higher Himalayan high-grade metasedimentary sequence, mainly garnet-bearing mica schists and gneisses. Higher Himalayan rocks close to the western edge of the KW form a klippe with a southwest-verging MCT at its' base. The KT, southern structural boundary of the window margin accommodating the differential exhumation between window internal and surroundings, is expressed as highly deformed sub-vertical shear bands.

Along the traverse of the Chenab River through the KW and further downstream, two prominent stretches along the Chenab River ~20 and ~25-30 km length are characterized by steep channel gradient associated with a large number of rapids (Fig.3b). These steep segments

362 are also characterized by a very narrow channel width (< 30m) (Fig.3b, 3e). The steepened
363 segments define knickzones (KZ) rather than single knickpoint (KP). The knickzone KZ1 in the
364 trunk stream as well as in the tributaries is hosted over bedrock gorge. Although the knickzone
365 KZ2 pass through a series of old landslides (around Kishtwar town), the rapids have all formed
366 in a bedrock channel. Therefore, neither KZ1 nor KZ2 appears to be related to damming by
367 recent landslides or other mass movements. The eastern margin of the KW is characterized by a
368 wide 'U-shaped' valley filled with thick sand layers and coarser fluvioglacial sediments (Fig. 3a)
369 where the Chenab River incises through this Late Pleistocene fill at present.

370 The rock strength data taken along the Chenab trunk stream portray large variations (R-
371 value ranging from 28 to 62) across different morphotectonic segments (fig. 7e). Within the KW,
372 Lesser Himalayan phyllites and schists have low R values (30-35); however, the low-strength
373 schists and phyllites are sparsely present and therefore are ignored when plotting the regional
374 rock strength values in fig. 7e. The dominant Lesser Himalayan quartzites in KW, as well as the
375 granitic intrusives in the eastern part of the KW, show very high R values of 55-62 and 51-56
376 respectively (fig. 7e). Compared to the high R values in the KW, the Higher Himalayan
377 metasediments show low strength (R: 35-45) till the point KP5 (fig. 3b). However, near the
378 western margin of the KW, the migmatites of Higher Himalayan domain show high rock strength
379 (R value: 58±3) (fig. 7e). The rock strength increases within the Haimanta Formation (R: 44±2)
380 further downstream until it reaches the MCT shear zone at the southern boundary of the Main
381 Himalayan orogen. The R-value in the frontal Lesser Himalaya is moderate (R: 41±2).

382 The Higher Himalayan sequence dips steeply away from the duplex (~65° towards west)
383 (fig. 2a, 8a*)*. The frontal nappes of the Lesser Himalaya expose internally-folded greenschist
384 facies rocks. Although at the western margin of the duplex, the quartzites stand sub-vertically,

the general dip amount reduces as we move from west to east for the next ~10-15 km (fig. 8). Near the core of the KW, we observed deformed quartz veins of at least two generations, as well as macroscopic white mica. Near the core of the window, where the river is also very steep and narrow, the rock units are also steeply-dipping towards the east (~60-65°) and are nearly isoclinal and vigorously deformed at places (fig. 2d, 2e). Towards the eastern edge of the window, however, the quartzites dip much more gently towards the east (~25-30°) and much lesser folding and faulting have been recognized in the field.

The E-W traverse of the Chenab River is completely devoid of any sediment storage. However, along the N-S traverse parallel to the western margin of the KW, ~150-170m thick sedimentary deposits are transiently-stored over the steeply-dipping Higher Himalayan bedrock. Norin (1926) argued the sediment aggradation in and around the Kishtwar town is largely contributed by fluvioglacial sediments and the U-shaped valley morphology is a marker of past glacial occupancy. We partially agree to the findings of Norin (1926) and Ul Haq et al., (2019) as we observe >100m thick fluvioglacial sediment cover unconformably overlying the Higher Himalayan bedrock along the N-S traverse of the Chenab River. The fluvioglacial sediments included alternate layers of pebble conglomerate and coarse-medium sand. The pebbles are moderately rounded and polished suggesting significant fluvial transport. Our field observations suggest that the fluvioglacial sediments have been succeeded by a significant volume of hillslope debris. The thickness of the debris-flow deposits is variable. The hillslope debris units contain mostly coarse-grained, highly-angular, poorly-sorted quartzite clasts from the frontal horses of the Lesser Himalayan Duplex. The town of Kishtwar is situated on this debris flow deposit (fig. 9). Along the N-S traverse of the Chenab, we have observed at least two epigenetic gorges lying along the main channel (fig. 3d). The active channel has incised the Higher Himalayan bedrock

and formed strath surfaces. We have identified at least three strath surface levels above the present-day river channel, viz., T1 (280±5 m), T2 (170-175 m) and T3 (~120±5 m), respectively (fig. 3g, 10a).

4.2. Results from morphometric analysis

4.2.1. Steep stream segments and associated knickpoints

The longitudinal stream profile along the Chenab River does not portray a typical adjusted concave-up profile across the Himalaya (fig. 6). We observe breaks in slope and concavity at several locations within a ~150 km traverse upstream from the MBT across the KW. These breaks are defined as knickpoints. Starting from the eastern margin of the KW till the MBT in the downstream, we identified at least six (6) discrete knickpoints in the river profile (fig. 6). Those are named KP1–KP6 according to their decreasing elevations. The upstream head of KZ1 and KZ2 are marked as KP2 and KP3, respectively (fig. 6). The slope breaks define the upstream reaches of the steep stream segments. The basinwide steepness indices span from ~30->750 $m^{0.9}$ across the study area (fig. 5d). We assigned a threshold value of k_{sn}>550 for the steepest watersheds/ stream segments. Along the traverse, the major knickpoints are KP1 (~1770m), KP2 (~1700m), KP3 (~1150m) and KP5 (~800m) respectively (fig. 6). Two minor knickpoints are there- KP4 (~1000m) and KP6 (~650m).

Already Nennewitz et al., (2018) had proposed a high basin-averaged k_{sn} value of > 300 in the KW. Here in this study, we worked with a more-detailed DEM and stream-specific k_{sn} allocation (fig. 7d), as well as a basinwide steepness calculation. Our results corroborate the earlier findings, but predict the zone of interest in greater detail. It is important to note that by setting a higher tolerance level in the 'knickpointfinder' tool in Topotoolbox, we have managed to remove the DEM artifacts from consideration (Schwanghart and Scherler, 2014).

4.2.2. Channel width and valley morphology

The channel width of the Chenab River is on average low (30-60m) within the core of the KW (fig. 3b, 7b), and the low channel width continues till the Chenab River flows N-S along the western margin of the KW. However, there are a few exceptions; upstream from the knickpoint KP1 in the Padder valley (in which the town of Padder is located), the channel widens (width ~80-100m) and the channel gradient is low (fig. 3a). The second instance of a wider channel is seen upstream from knickpoint KP3, where there is a reservoir for the Dul-Hasti dam. Downstream from KP3 within the Higher Himalaya, the channel width ranges from 50-70 m. However, towards the lower stretches of the N-S traverse, the width is even lower (16-52m). The river width increases to 100-200m as Chenab River takes a westward path thereafter. The channel width increases beyond 300m until it leaves the crystalline rocks in the hanging wall of the MCT and enters the Lesser Himalaya in the hanging wall of the MBT across the Baglihar dam. Within the frontal LH, the channel width is again lowered (50-80 m).

4.2.3. Changes in specific stream power (SSP)

Discharge-normalized SSP data calculated from the upstream stretches and the knickzones, KZ1 and KZ2, show major increase in SSP within the steep knickzones. The increase in SSP from upstream to the knickzones KZ1 and KZ2 are 4.44 and 5.02 times, respectively (Table 1). Such high increase in SSP is aided by steepening of channel gradient (fig. 7c) and narrowing of channel bed (fig. 7b).

4.3. Luminescence chronology

The results for the luminescence chronology are listed in Table 2. Samples collected from the fluvioglacial sediments overlain by debris flow deposit, namely as, K07, K08 and K09, yield IRSL ages of 104.5±5.9 kyr, 114.4±6.3 kyr, and 119.2±6.8 kyr, respectively. Fading corrections

done for samples K07 and K09 yield the correction factors (g%) of 0.89 and 1.11 respectively. The sample K08 has not been treated for fading correction, but for easier understanding, we have assumed a constant sedimentation rate between the samples K07 and K09 and extrapolated the 'fading-corrected' age for K08. The oldest sample K09 (132±7 kyr) (fading-corrected IRSL age) is succeeded by samples K08 (126±6 kyr) and K07 (113±6 kyr) respectively. The finer fraction of the hillslope debris overlying the fluvio-glacial deposits yield OSL ages of 81.1±4.6 kyr (K02) and 85±5 kyr (K11) (Fig.6). OSL samples taken from sparsely-preserved sediment layers above the T3 strath surface shows heterogeneous bleaching and hence we provide a minimum age of 22.8±2.1 kyr (sample K16) and 20.5±1.0 kyr (sample K17). One sample taken above T1 strath level is saturated and shows a minimum age of 52.1±2.8 kyr (sample K18) (Table 2). OSL samples K01 and K06 taken from sand layers sitting atop the Higher Himalayan bedrock straths near the town of Doda portray depositional ages of 49.8±2.9 kyr and 51.6±2.4 kyr, respectively (Table 2).

5. Discussions

Analysis of morphometric parameters are widely used as indicators of active tectonics and transient topography (Kirby and Whipple, 2012; Seeber and Gornitz, 1983). Many studies have used morphometry as a proxy for understanding the spatial distribution of active deformation across certain segments of the Himalayan front (Malik and Mohanty, 2007; van der Beek et al., 2016; Nennewitz et al., 2018; Kaushal et al., 2017). More importantly, some studies have integrated morphometric analysis with chronological constraints to assess the spatial and temporal variability in deformation within the Sub-Himalaya (Lave and Avouac, 2000; Thakur et

al., 2014; Vassalo et al., 2015; Dey et al., 2016; Srivastava et al., 2018). All these studies have demonstrated the applicability of morphometric indicators as an estimate of changes in uplift rate or spatial variations of deformation across different landscapes.

Previously-published young apatite fission-track cooling ages (~ 2-3 Myr) have been interpreted as the result of rapid exhumation of the LH duplex over 10^6-year timescale (Gavillot et al., 2018). However, how and where the deformation is accommodated across the KW over the 10^3-10^5-year timescale is unknown. In this section, we discuss the obtained morphometric and fluvial characteristics of the studied region and compare these to existing models of deformation. We also discuss how our new luminescence chronological estimates from the transiently-stored sediment archive help us to constrain fluvial incision rates over Late Pleistocene- Holocene timescale and put them in context to regional tectonic deformation models- 1. Mid-crustal ramp model vs. 2. Out-of-sequence fault model.

5.1. Knickpoints and their genesis

Already Seeber and Gornitz (1983) had recognized that the Chenab River is characterized by a zone of steep channel gradient in the vicinity of the KW. Nennewitz et al. (2017) demonstrated a strong correlation between steeped longitudinal river profiles and young thermochronological cooling ages, suggesting recent focused rock uplift and rapid exhumation along many major rivers draining the southern Himalayan front. However, it is still an open debate whether uplift and growth of the LH Duplex are triggered solely by slip over the crustal ramp of the MHT or additional out-of-sequence surface-breaking faults augmenting it (Herman et al., 2010; Elliot et al., 2016; Whipple et al., 2016).

499 The longitudinal profile of the lower Chenab traverse (below ~2000 m above MSL) is
500 punctuated by two prominent stretches of knickpoint zones and several minor knickpoints related
501 to change of fluvial gradient (fig. 6). Below we will discuss the potential cause of formation of
502 those major knickpoints in the context of detailed field observation, existing field-collected
503 structural and lithological data, geomorphic features, rock strength and channel width
504 information (fig. 7).

505 ***5.1.1. Lithologically-controlled knickpoints***

506 Our findings show that the Himalayan traverse of the Chenab River is characterized by
507 large variations in substrate lithology and rock strength, which cause variations in the fluvial
508 erodibility and form knickpoints on the river profile (fig. 1, fig. 7e). An instance of soft-to-hard
509 substrate transition happens across the knickpoint KP1, lying downstream from the Padder
510 valley, at the eastern edge of the KW (fig. 2a). Across KP1, the river enters the over-deepened
511 LH bedrock gorge (R value> 50) after exiting the Padder valley filled with transiently-stored,
512 unconsolidated fluvioglacial sediments (fig. 3a). A similar soft-to-hard substrate transition is
513 observed upstream from the MCT shear zone. The corresponding knickpoint KP5 represents a
514 change in lithological formation from the sheared and deformed Higher Himalayan crystalline (R
515 value~35-40) to deep-seated Haimantas (R value~40-50). There is no field evidence, such as
516 fault splays or ramps, in support of KP5 being structurally-controlled.

517 ***5.1.2. Tectonically-controlled knickpoints***

518 Compiling previously-published data on regional tectonogeomorphic attributes (Gavillot
519 et al., 2018) with detailed field documentation of structural styles and tectonic features, we
520 identified several stretches where variations in morphometric proxies indicate spatial variability
521 in rock uplift and faulting across the KW. We have found at least two instances where

knickzones are not related to change in substrate, nor are they artificially altered such as constructed dam sites.

The knickzone KZ1 (upstream marked by KP2 ~1700 m above MSL) represents the upstream reach of a steepened river-segment that represents a drop of ~420m of the Chenab River across a run-length of ~15-20 km (fig. 8c). The upstream and downstream side of KP2 is characterized by a change in dip of the LH bedrock foliation (fig. 2f, 2g, 8) and channel width (fig. 7b). KP2 also reflects a change in the channel width (fig. 7b). Interestingly, the steep segment exhibits a narrower channel and particularly steep valley-walls through the core of the KW. Near the end of the steep segment, intensely-deformed (folded and fractured) LH rocks are exposed (fig. 2d, 2e). We infer two main possibilities for these field observations combined with systematic changes of geomorphic characteristics – (1) it may be related to an active surface-breaking out-of-sequence fault or (2) it may be an inactive fault that defines the floor-thrust of one of the numerous proposed duplex nappes. The observed changes in the geomorphic indices along with stretch of the knickzone KZ1 and observed increase in the bedrock dip angle may well be explained by a ramp on the basal decollement. This explanation is supported by the existence of mid-crustal ramps in the balanced cross-section from Gavillot et al. (2018). However, the structural orientation of the rocks (Fig.8a) differ considerably from those of the proposed LH duplex in Gavillot et al. (2008) raising questions about the duplex-model. Our field observations are supported by previous studies by Fuchs (1975), Frank et al. (1995) and Stephenson et al. (2000) who argued against duplexing of multiple thrust nappes and favoured internal folding of Chail nappe to explain the tectonic growth and deformation pattern within the KW. Therefore, we cannot clearly comment whether K1 represents a transition from flat to ramp of the MHT or is it indeed an active out-of-sequence thrust-ramp.

On the other hand, the other knickpoint KP3 at the upstream-head of KZ2 nearly coincides with the exposure of the KT (fig. 6). KP3 cannot be a lithologically-controlled knickpoint as it reflects a hard-to-soft substrate transition from LH rocks (R value> 50) to HH rocks (R value< 45) (fig. 7e). We acknowledge that just across the point KP3, there are some strong leucosomatic layers within the migmatites (R: 58±3), but in general, the migmatites are also brittle-deformed. The rock strength measurement was not done in the multiply-fractured units as it would show inaccurate values. In the longitudinal profile, KP3 does not represent a sharp slope break because the downstream segment runs parallel to main structures and KW-boundary for ~25-30 km, including the KT. Therefore, we performed an orthogonal projection of the E-W trending traverses of the Chenab River and estimated an orogen-perpendicular drop of the Chenab across KZ2 (fig. 8c). The truncated profile across KZ2 shows a drop of ~230m of the channel across an orogen-perpendicular run-length of ~5 km. The orogen-parallel stretch of the river exhibits narrow channel width (<30-35m) through moderately hard HH bedrock (R-value: 35-45). The tributaries within this stretch form a significant knickpoint at the confluence with the trunk stream (fig. 3f). These field observations suggest recent rapid uplift of the western margin of the KW. The observed differential uplift of the KW margin is possibly either related to growth of the LH-duplex in the core of the window or surface expression of another crustal ramp emerging from the MHT (fig. 8d). Both the knickzones, KZ1 and KZ2 are the most-prominent disturbance in the longitudinal profile of the Chenab River and are interpreted to portray spatial distribution of differential uplift due to tectonic deformation.

5.2. Temporal and spatial variation of fluvial incision across the KW

Bedrock incision in the Himalaya is not a continuous process and is rather controlled by temporal variations in sediment flux that usually dictates the thickness of the veneer above the

bedrock surfaces over which the rivers flow. Late Pleistocene-Holocene sediment transport studies suggested an overall climatic control on sediment aggradation in the interiors of the Himalayan orogen (e.g., Bookhagen et al., 2005; Scherler et al., 2015; Dey et al., 2016); where, stronger climatic conditions may increase the sediment supply and prompt filling of a river valley. Transiently-stored valley-fills are re-incised once the climate weakens. Often the re-incision phases dissect the bedrock units and form strath surfaces. In Chenab valley, we have documented several stages of valley-fills and fluvial strath surfaces.

5.2.1. Sediment aggradation in Chenab valley

The Chenab valley records a net sediment aggradation and transient filling of entire drainage network in the vicinity of the KW since the onset of the last glacial-interglacial cycle (~130 kyr) till ~80 kyr. Fluvioglacial outwash sediments range from at least ~110-130 kyr, whereas the hillslope debris ranges from ~90 to ~80 kyr (Table 2). The chronology of the sediments is in agreement with the overall stratigraphic order of the sediments across the KW. We observe net fluvial re-incision and formation of bedrock strath surfaces since ~80 kyr and formation of epigenetic gorges (fig. 10).

5.2.2. Drainage re-organization and strath terrace formation along Chenab River

Hillslope debris flow from the high-relief frontal horses of the Lesser Himalayan Duplex overlies the fluvio-glacial sediments stored beneath the Kishtwar surface. We argue that the hillslope debris is from paleo-landslide deposits which intervened and dammed the paleo-drainage of the Chenab River, which might have been flowing through an easterly path than now (fig. 9). The Maru River, coming from the northwestern corner of our study area was also joining the Chenab River at a different location (fig. 9). Our argument is supported by field observation of thick silt-clay layer in the proposed paleo-valley of the Maru River (fig. 9a, 9c). OSL sample

591 K18 from the silt-clay layer is saturated and hence only provides the minimum age of 52±3 kyr.
592 We suggest that the hillslope sediment flux dammed the flow of the Chenab River and also
593 propagated through the aforesaid wind-gap of the Maru River. The decline in the depositional
594 energy resulted in reduction of grain-size. Post-hillslope debris flow, the Chenab River also
595 diverted to a new path. The new path of the Chenab River upstream from the confluence with the
596 Maru River is defined by a very narrow channel flowing through the Higher Himalayan bedrock
597 gorge (fig. 7b). Downstream from the confluence, we are able to identify at least three levels of
598 strath terraces lying at heights of ~280-290m (T1), ~170m (T2) and ~120m (T3), respectively
599 (fig. 3g,10a). Our field observation suggests that the formation of the straths is at least ~52 kyr-
600 old. The luminescence chronology samples in this study belong to the ~150-170m-thick soft
601 sediments that are stored stratigraphically-up from the T1 strath level. Our field observations and
602 chronological estimates suggest that the renewed path of the Chenab River, must have been
603 formed post the hillslope debris flow ~80-90 kyr but before 52 kyr.

604 ***5.2.3. Knickpoint marking epigenetic gorge***

605 Epigenetic gorges are common geomorphic features in the high-mountain landscape
606 (Ouimet et al., 2008). Epigenetic gorges form when channels of a drainage system are transiently
607 buried by sediment aggradation and during subsequent re-incision, a new river channel, often
608 into the neighbouring bedrock is incised. The N-S traverse of the Chenab River is largely
609 affected by hillslope sediment flux (paleo-landslides and debris flow) from the steep eastern
610 flank. The knickpoint KP4, situated near the village of Janwas, marks one such instance of an
611 epigenetic gorge where the paleo-valley has been filled initially by fluvioglacial sediments and
612 the channel abandonment was caused by landslides and hillslope debris flow prior to 80 kyr (fig.
613 4b, 4c).

614

615 **5. 3. Rapid bedrock incision along Chenab River on Late Pleistocene timescale**

616 Considering the rate of excavation of softer sediments to be at least an order of magnitude
617 higher than the rate of bedrock incision (Kothyari and Juyal, 2013; Sharma et al., 2016), we
618 calculated the minimum bedrock incision rate at the western margin of the KW, using the height
619 of the T1 strath (~280±5 m) and the average age of the sediments from the Hillslope debris flow
620 deposit. It yields a minimum bedrock incision rate of ~3.1-3.5 mm/yr over the last 80-90 kyr.
621 Considering the saturated OSL sample from the paleo-valley, we estimated the maximum
622 bedrock incision since 52 kyr to be 5.1-5.5 mm/yr. Similarly, using the minimum age estimate of
623 the T3 terrace abandonment, we deduce a maximum bedrock incision rate of ~5.7-6.1 mm/yr
624 since ~21 kyr. However, further downstream, away from the KW, the average bedrock incision
625 rate derived from dated strath surfaces (~36±2 m high from the Chenab River) near the town of
626 Doda is 0.7±0.1 mm/yr (sample K01 and K06). We do not have bedrock incision rates from the
627 core and the eastern margin of the KW, as the core is devoid of sediment storage and the eastern
628 margin is filled with fluvioglacial sediments and the river is incising the fill. Nonetheless, these
629 results indicate that despite transient choking of the drainage network by sediments during times
630 of valley aggradation, the topography experienced high incision, when sediment coverage had
631 been completely penetrated and bedrock straths had been created post-renewal of the fluvial
632 flow.

633

634 **5.4. Our new results in context with the previously-published data**

635 AFT-cooling ages by Kumar et al., (1995) showcased young cooling ages from the core
636 of the KW and its western margin (AFT ages: ~2-3 Myr) compared to the surroundings (AFT

637 age: 6-12 Myr). The calculated high exhumation rates proposed by Gavillot et al., (2018) are
638 based on using a geothermal gradient of 35-40˚C/km in Dodson's equation assuming a 1-D
639 model (Dodson, 1973). Additional data and thermal modeling are needed across the KW to
640 constrain the exhumation rates from vertical transects. However, lateral similarities of the
641 regional topography and age patterns along the Sutlej area, in the Beas valley and the Dhauladhar
642 Range (Thiede et al., 2017; Thiede et al., 2009; Stübner et al., 2018), have yielded similar
643 exhumation rates in the range of 2-3 mm/yr. Long-term exhumation rates from the NW
644 Himalaya agree well with findings of Nennewitz et al. (2018) who correlated the young
645 thermochron ages with high basinwide k_{sn} values suggesting high uplift rates over intermediate
646 to longer timescales. Although the geomorphic implications on landscape evolution provide
647 resolution at shorter timescales than the low-T thermochron studies, our field observations and
648 analysis support very well a protracted long-term uplift rates across the KW. Interestingly,
649 exhumation rates in the steepened stretches are nearly one order of magnitude higher than that of
650 the Higher Himalayan units in the klippe. Our estimates of SSP also reflect an increase by ~five
651 times within the steepened stretches.

652 **5.5. Two competing models: duplex-growth model vs. out-of-sequence fault-ramp model**

653 Deeply-incised channel morphology and steep channel gradients marked by knickpoints
654 at the upstream reaches in and around the KW could be explained by the presence of at least two
655 orogen-parallel mid-crustal ramps on the MHT (fig. 8d). Existence of two mid-crustal ramps has
656 already been shown through sequential balanced cross-sections for the last 10 Myr across the
657 Kashmir Himalaya (Gavillot et al., 2018). The study by Gavillot et al., (2018) focused on duplex
658 growth model as the balanced cross-section portrays several LH nappes stacked together (fig.
659 8d). Translation on the MHT can impart differential uplift of the LH duplex across the two mid-

660 crustal ramps as ramps would show higher uplift/ exhumation due to higher angle of dip of floor-
661 thrust of the duplex. Here we provide more detailed information on spatial distribution of active
662 differential uplift across the KW (fig. 8a, 8d). Our field observation questions the existence of
663 multiple nappes forming a duplex (Gavillot et al., 2018) and rather favors anticlinal doming of
664 the pervasively-deformed Chail nappe, as suggested by Fuchs (1975) and Stephenson et al.,
665 (2000). We observe pronounced deformation at the core of the KW (fig. 2d, 2e) suggesting that
666 this could be related to active faulting, crustal buckling or internal folding which maintain
667 continuous rock-uplift forcing the Chenab River to incise and maintain the steepened stretch of
668 KZ1. Gavillot et al. (2018) proposed that translation on a mid-crustal ramp of the MHT and no
669 surface-faulting is driving the uplift at the core of the KW (fig. 8d). We provide an alternative
670 explanation for the observed steep stream segment at the core of the KW. We speculate the
671 existence of a crustal fault-ramp emerging from the MHT that triggers rapid exhumation of the
672 hanging wall. In that case, out-of-sequence faulting causes high relief, steep channel gradients
673 and higher basinwide steepness indices over the ramp (fig. 7). Similar ramps have been proposed
674 on the MBT beneath the Dhauladhar Range (Thiede et al., 2017) and in the east of the NW
675 Himalaya (Caldwell et al., 2013; Mahesh et al., 2015; Stübner et al., 2018; Yadav et al., 2019).
676 Similar mid-crustal ramp (MCR-2) has been proposed for the western margin of the KW by
677 Gavillot et al., (2018). We do not have any direct field evidence of regional surface-breaking
678 faults which could be related to KZ2. However, rapid fluvial incision, increase in SSP and
679 channel steepness probably justify the existence of either a mid-crustal ramp or an out-of-
680 sequence surface-breaking fault.

681 Detailed structural mapping and morphometric analysis using high-resolution DEM
682 provide important constraints on the spatial extent of deformation. We are able to resolve the

683 high-relief Kishtwar Window and the surroundings into two major steep orogen-parallel belts/
684 zones (fig. 5e, 8d) - one at the core of the KW could be an active high-angle fault-ramp emerging
685 from the MHT or a crustal ramp, and the other observed along the western margin of the KW
686 could be another ramp on the MHT or a surface-breaking back-thrust evolving in relationship to
687 the growth of the LH duplex. More importantly, we demonstrate that the Kishtwar Window is
688 still growing and therefore could be the potential source of future seismic activity.
689
690 **6. Conclusions**
691
692 Our field observation and the characteristics of terrain morphology match well with the
693 spatial pattern of previously-published thermochronological data and indicate that the Kishtwar
694 Window is undergoing tectonic deformation, uplift and exhumation at present, on Late
695 Pleistocene-Holocene timescales, and in geological past since at least the late Miocene. By
696 compiling our new results and published records, we favor the following conclusions:
697 1. The Chenab River maintains an over-steepened bedrock channel and a low
698 channel width irrespective of lithological variations across the KW and beyond,
699 suggesting ongoing rapid fluvial incision related to active tectonic rock uplift.
700 2. Our field observations, morphometric analysis, and rock strength measurements
701 document that at least two of these major knickzones with steep longitudinal
702 gradients on the trunk stream are non-lithologic and are likely related to
703 differential rock uplift. The incision potential (specific stream power) in the
704 steepened stretches ~4-5 times higher than the surroundings.

3. The differential uplift can be explained either by slip on the multiple ramps on the MHT and exhumation of the duplex floor-thrust or by a combination of slip on the MHT ramp and active out-of-sequence faulting. As of now, we do not have any evidence for large-scale out-of-sequence faulting.
4. Luminescence chronology of the transiently-stored sediments along the Chenab River suggests that the valley had been overfilled by sediments of fluvio-glacial origin as well as by hillslope sediment flux. Massive sediment aggradation during ~130-80 kyr led to drainage re-organization and bedrock incision leaving behind strath surfaces.
5. The late Quaternary bedrock incision rates near the western margin of the KW are high 3.1-3.6 mm/yr while away from KW, the incision rates are low (< 1 mm/yr).

To summarize, our new study reinforces the importance of detailed field observation, and morphometric analysis in understanding the neotectonic framework of the interiors of the Himalaya. With additional chronological evidence from the transiently-stored sediments, we showcase high rates of bedrock incision in the interior of the western Himalaya, which could potentially be indicative of tectonic control on landscape evolution. However, to solve the debate of ongoing duplex-growth vs. active out-of-sequence faulting, we would require more field data on active structures and chronological constraints on deformation rates across potentially-active structures.

Appendix

Additional maps, figures on morphometric analysis and luminescence dating are listed in Appendix A. Data of rock strength measurements provided in Table C1. Luminescence sample processing is elaborated in Appendix B.

Code availability

Authors used open-source codes of Topotoolbox and Topographic Analysis Kit Toolbox for this study.

Data availability

Field data are already provided in Appendix 1. Additional data on luminescence dating can be provided on request.

Sample availability

Samples used for luminescence dating are already mostly-destroyed, therefore it is beyond sharing.

Author contribution

S.Dey, the first author, led this work and completed the fieldwork, sample processing, measurements and writing of this manuscript. R. Thiede helped in fieldwork, discussion and writing of this manuscript. A. Biswas performed the initial morphometric analysis. N. Chauhan helped in measurement of luminescence signal and assessment of the data. P. Chakravarti performed the channel width calculations and compiled the rock strength measurements. V. Jain helped in discussion and writing of the manuscript.

Competing interests

The authors declare that they have no conflict of interest.

Acknowledgments

This study is funded by the DST INSPIRE faculty fellowship program by the Department of Science and Technology, India (grant #DST/INSPIRE/04/2017/003278), and IIT Gandhinagar post-doctoral research fund (IP/IITGN/ES/SD/201718-01). Thiede is supported by German

751 Science Foundation (grant # DFG TH 1317-8 and 9). We thank M.K.Jaiswal and M.Rawat for
752 providing the elemental analysis. We thank Shambhu Das, Avi Das, Niklas Schaaf, Akashsingh
753 Rajput and Chamel Singh for their assistance during fieldwork. We also thank Soumyajit
754 Mukherjee, Rahul Kaushal and Shantamoy Guha for scientific inputs and comments on this
755 manuscript. We acknowledge A. Forte, Y. Gavillot, S. Hergarten and one anonymous reviewer
756 for their constructive and insightful reviews. We like to thank the editors R. Gloaguen and A.
757 Joshua West for their generous help during review process.

758

759 **References**

760 Abrahami, R., van der Beek, P., Huyghe, P., Hardwick, E., & Carcaillet, J. (2016). Decoupling of
761 long-term exhumation and short-term erosion rates in the Sikkim Himalaya. Earth and Planetary
762 Science Letters, 433, 76-88.

763 Bagnold, R. A. (1966). An approach to the sediment transport problem from general physics. US
764 government printing office.

765 Bhatia, T. R., & Bhatia, S. K. (1973). Sedimentology of the slate belt of Ramban-Banihal area,
766 Kashmir Himalaya. Himalayan Geology, 3, 116-134.

767 Bollinger, L., Henry, P., & Avouac, J. P. (2006). Mountain building in the Nepal Himalaya:
768 Thermal and kinematic model. *Earth and Planetary Science Letters*, *244*(1-2), 58-71.

769 Bookhagen, B., & Burbank, D. W. (2006). Topography, relief, and TRMM-derived rainfall
770 variations along the Himalaya. Geophysical Research Letters, 33(8).

771 Bookhagen, B., Thiede, R. C., & Strecker, M. R. (2005). Late Quaternary intensified monsoon
772 phases control landscape evolution in the northwest Himalaya. *Geology*, *33*(2), 149-152.

773 Bookhagen, B., Fleitmann, D., Nishiizumi, K., Strecker, M. R., & Thiede, R. C. (2006).
774 Holocene monsoonal dynamics and fluvial terrace formation in the northwest Himalaya,
775 India. *Geology*, *34*(7), 601-604.

776 Burbank, D. W., Leland, J., Fielding, E., Anderson, R. S., Brozovic, N., Reid, M. R., & Duncan,
777 C. (1996). Bedrock incision, rock uplift and threshold hillslopes in the northwestern
778 Himalayas. *Nature*, *379*(6565), 505.

779 Burgess, W. P., Yin, A., Dubey, C. S., Shen, Z. K., &Kelty, T. K. (2012). Holocene shortening
780 across the Main Frontal Thrust zone in the eastern Himalaya. Earth and Planetary Science
781 Letters, 357, 152-167.

782 Caldwell, W. B., Klemperer, S. L., Lawrence, J. F., and Rai, S. S., 2013, Characterizing the Main
783 Himalayan Thrust in the Garhwal Himalaya, India with receiver function CCP stacking: Earth
784 and Planetary Science Letters, v. 367, p. 15-27.

785 Colleps, C. L., Stockli, D. F., McKenzie, N. R., Webb, A. A. G., & Horton, B. K. (2019).
786 Neogene Kinematic Evolution and Exhumation of the NW India Himalaya: Zircon Geo-and
787 Thermochronometric Insights From the Fold-Thrust Belt and Foreland Basin. Tectonics, 38(6),
788 2059-2086.

789 DeCelles, P. G., Robinson, D. M., Quade, J., Ojha, T. P., Garzione, C. N., Copeland, P., and
790 Upreti, B. N., 2001, Stratigraphy, structure, and tectonic evolution of the Himalayan fold-thrust
791 belt in western Nepal: Tectonics, v. 20, no. 4, p. 487-509.

792 Deeken, A., Thiede, R. C., Sobel, E. R., Hourigan, J. K., & Strecker, M. R. (2011).
793 Exhumational variability within the Himalaya of northwest India. Earth Planetry Science Letters,
794 305(1-2), 103–114. https://doi.org/10.1016/j.epsl.2011.02.045

795 Dey, S., Thiede, R. C., Schildgen, T. F., Wittmann, H., Bookhagen, B., Scherler, D., & Strecker,
796 M. R. (2016). Holocene internal shortening within the northwest Sub-Himalaya: Out-of-
797 sequence faulting of the Jwalamukhi Thrust, India. Tectonics, 35(11), 2677-2697.

798 Dey, S., Thiede, R. C., Schildgen, T. F., Wittmann, H., Bookhagen, B., Scherler, D., Jain, V., &
799 Strecker, M. R. (2016). Climate-driven sediment aggradation and incision since the late
800 Pleistocene in the NW Himalaya, India. *Earth and Planetary Science Letters*, *449*, 321-331.

801 DiPietro, J. A., & Pogue, K. R. (2004). Tectonostratigraphic subdivisions of the Himalaya: A
802 view from the west. Tectonics, 23(5).

803 Duvall, A., Kirby, E., & Burbank, D. (2004). Tectonic and lithologic controls on bedrock
804 channel profiles and processes in coastal California. Journal of Geophysical Research: Earth
805 Surface, 109(F3).

806 Elliott, J. R., Jolivet, R., González, P. J., Avouac, J. P., Hollingsworth, J., Searle, M. P., &
807 Stevens, V. L. (2016). Himalayan megathrust geometry and relation to topography revealed by
808 the Gorkha earthquake. *Nature Geoscience*, *9*(2), 174.

809 Eugster, P., Scherler, D., Thiede, R. C., Codilean, A. T., and Strecker, M. R., (2016). Rapid Last
810 Glacial Maximum deglaciation in the Indian Himalaya coeval with midlatitude glaciers: New
811 insights from 10Be-dating of ice-polished bedrock surfaces in the Chandra Valley, NW
812 Himalaya: Geophysical Research Letters, v. 43, no. 4, p. 1589-1597.

813 Finnegan, N. J., Roe, G., Montgomery, D. R., &Hallet, B. (2005). Controls on the channel width
814 of rivers: Implications for modeling fluvial incision of bedrock. *Geology*, *33*(3), 229-232.

Flint, J. J. (1974). Stream gradient as a function of order, magnitude, and discharge. Water Resources Research, 10(5), 969-973.

Forte, A.M. and Whipple, K.X. (2019). The Topographic Analysis Toolkit (TAK) for Topotoolbox. Earth Surface Dynamics, 7, 87-95.

Frank, W., Grasemann, B., Guntli, P. E. T. E. R., & Miller, C. (1995). Geological map of the Kishtwar-Chamba-Kulu region (NW Himalayas, India). Jahrbuch der Geologischen Bundesanstalt, 138(2), 299-308.

Fuchs, G. (1975). Contributions to the geology of the North-Western Himalayas. Geologische Bundesanstalt.

Fuchs, G. (1981). Outline of the geology of the Himalaya. Mitt. osterr. geol. Ges, 74(75), 101-127.

Gavillot, Y. G. (2014). Active tectonics of the Kashmir Himalaya (NW India) and earthquake potential on folds, out-of-sequence thrusts, and duplexes.

Gavillot, Y., Meigs, A. J., Sousa, F. J., Stockli, D., Yule, D., & Malik, M. (2018). Late Cenozoic Foreland-to-Hinterland Low-Temperature Exhumation History of the Kashmir Himalaya. Tectonics.

Gavillot, Y., Meigs, A., Yule, Y., Heermance, R., Rittenour, T., Madugo, C., & Malik, M. (2016). Shortening rate and Holocene surface rupture on the Riasi fault system in the Kashmir Himalaya: Active thrusting within the Northwest Himalayan orogenic wedge. Geological Society of America Bulletin, 128(7-8), 1070–1094. https://doi.org/10.1130/B31281.1

Harvey, J. E., Burbank, D. W., & Bookhagen, B. (2015). Along-strike changes in Himalayan thrust geometry: Topographic and tectonic discontinuities in western Nepal. Lithosphere, 7(5), 511-518.

Herman, F., Copeland, P., Avouac, J.P., Bollinger, L., Mahéo, G., Le Fort, P., Rai, S., Foster, D., Pêcher, A., Stüwe, K. and Henry, P., 2010. Exhumation, crustal deformation, and thermal structure of the Nepal Himalaya derived from the inversion of thermochronological and thermobarometric data and modeling of the topography. *Journal of Geophysical Research: Solid Earth*, *115*(B6).

Hirschmiller, J., Grujic, D., Bookhagen, B., Coutand, I., Huyghe, P., Mugnier, J.-L., and Ojha, T., 2014, What controls the growth of the Himalayan foreland fold-and-thrust belt?: Geology, v. 42, no. 3, p. 247-250.

Kaushal, R. K., Singh, V., Mukul, M., & Jain, V. (2017). Identification of deformation variability and active structures using geomorphic markers in the Nahan salient, NW Himalaya, India. *Quaternary International*, *462*, 194-210.

Kumar, A., Lal, N., Jain, A. K., &Sorkhabi, R. B. (1995). Late Cenozoic–Quaternary thermo-tectonic history of Higher Himalayan Crystalline (HHC) in Kishtwar–Padar–Zanskar region, NW Himalaya: Evidence from fission-track ages. Journal of the Geological Society of India, 45(4), 375–391.

Kundu, B., Yadav, R. K., Bali, B. S., Chowdhury, S., &Gahalaut, V. K. (2014). Oblique convergence and slip partitioning in the NW Himalaya: implications from GPS measurements. Tectonics, 33(10), 2013-2024.

Lavé, J., & Avouac, J. P. (2000). Active folding of fluvial terraces across the Siwaliks Hills, Himalayas of central Nepal. Journal of Geophysical Research: Solid Earth, 105(B3), 5735-5770.

Lavé, J., & Avouac, J. P. (2001). Fluvial incision and tectonic uplift across the Himalayas of central Nepal. Journal of Geophysical Research: Solid Earth, 106(B11), 26561-26591.

Mahesh, P., Gupta, S., Saikia, U., and Rai, S. S., 2015, Seismotectonics and crustal stress field in the Kumaon-Garhwal Himalaya: Tectonophysics, v. 655, p. 124-138.

Malik, J. N., & Mohanty, C. (2007). Active tectonic influence on the evolution of drainage and landscape: geomorphic signatures from frontal and hinterland areas along the Northwestern Himalaya, India. *Journal of Asian Earth Sciences*, *29*(5-6), 604-618.

Miller, J. R. (1991). The influence of bedrock geology on knickpoint development and channel-bed degradation along downcutting streams in south-central Indiana. The Journal of Geology, 99(4), 591-605.

Mitra, G., Bhattacharyya, K., & Mukul, M. (2010). The lesser Himalayan duplex in Sikkim: implications for variations in Himalayan shortening. *Journal of the Geological Society of India*, *75*(1), 289-301.

Montgomery, D. R., & Brandon, M. T. (2002). Topographic controls on erosion rates in tectonically active mountain ranges. Earth and Planetary Science Letters, 201(3-4), 481-489.

Mukherjee S. (2015) A review on out-of-sequence deformation in the Himalaya. In: Mukherjee S, Carosi R, van der Beek P, Mukherjee BK, Robinson D (Eds) Tectonics of the Himalaya. Geological Society, London. Special Publications 412, 67-109.

876 Nábělek, J., Hetényi, G., Vergne, J., Sapkota, S., Kafle, B., Jiang, M., Su, H., Chen, J., & Huang,
877 B. S. (2009). Underplating in the Himalaya-Tibet collision zone revealed by the Hi-CLIMB
878 experiment. Science, 325(5946), 1371-1374.

879 Nadim, F., Kjekstad, O., Peduzzi, P., Herold, C., &Jaedicke, C. (2006). Global landslide and
880 avalanche hotspots. Landslides, 3(2), 159-173.

881 Nennewitz, M., Thiede, R. C., & Bookhagen, B. (2018). Fault activity, tectonic segmentation,
882 and deformation pattern of the western Himalaya on Ma timescales inferred from landscape
883 morphology. Lithosphere, 10(5), 632-640.

884 Ni, J., and M. Barazangi (1984), Seismotectonics of the Himalayan collision zone: Geometry of
885 the underthrusting Indian plate beneath the Himalaya, J. Geophys. Res., 89, 1147 – 1163.

886 Powers, P. M., Lillie, R. J., & Yeats, R. S. (1998). Structure and shortening of the Kangra and
887 Dehra Dun reentrants, sub-Himalaya, India. Geological Society of America Bulletin, 110(8),
888 1010-1027.

889 Raiverman, V. (1983). Basin geometry, Cenozoic sedimentation and hydrocarbon prospects in
890 north western Himalaya and Indo-Gangetic plains. Petroleum Asia Journal: Petroliferous basins
891 of India, 6(4), 67-92.

892 Robert, X., Van Der Beek, P., Braun, J., Perry, C., Dubille, M., & Mugnier, J. L. (2009).
893 Assessing Quaternary reactivation of the Main Central thrust zone (central Nepal Himalaya):
894 New thermochronologic data and numerical modeling. *Geology*, *37*(8), 731-734.

Robinson, D. M., & Martin, A. J. (2014). Reconstructing the Greater Indian margin: A balanced cross section in central Nepal focusing on the Lesser Himalayan duplex. *Tectonics*, *33*(11), 2143-2168.

Royden, L., & Taylor Perron, J. (2013). Solutions of the stream power equation and application to the evolution of river longitudinal profiles. *Journal of Geophysical Research: Earth Surface*, *118*(2), 497-518.

Scherler, D., Bookhagen, B., Wulf, H., Preusser, F., & Strecker, M. R. (2015). Increased late Pleistocene erosion rates during fluvial aggradation in the Garhwal Himalaya, northern India. *Earth and Planetary Science Letters*, *428*, 255-266.

Schwanghart, W., &Scherler, D. (2014). TopoToolbox 2–MATLAB-based software for topographic analysis and modeling in Earth surface sciences. Earth Surface Dynamics, 2(1), 1-7.

Searle, M. P., Stephenson, B., Walker, J., & Walker, C. (2007). Restoration of the Western Himalaya: implications for metamorphic protoliths, thrust and normal faulting, and channel flow models. Episodes, 30(4), 242.

Seeber, L., &Gornitz, V. (1983). River profiles along the Himalayan arc as indicators of active tectonics. *Tectonophysics*, *92*(4), 335-367.

Snyder, N. P., Whipple, K. X., Tucker, G. E., &Merritts, D. J. (2000). Landscape response to tectonic forcing: Digital elevation model analysis of stream profiles in the Mendocino triple junction region, northern California. Geological Society of America Bulletin, 112(8), 1250-1263.

Steck, A. (2003). Geology of the NW Indian Himalaya. EclogaeGeolHelv, 96, 147-196.

915 Stephenson, B. J., Waters, D. J., & Searle, M. P. (2000). Inverted metamorphism and the Main
916 Central Thrust: field relations and thermobarometric constraints from the Kishtwar Window, NW
917 Indian Himalaya. Journal of Metamorphic Geology, 18(5), 571-590.

918 Stevens, V. L., & Avouac, J. P. (2015). Interseismic coupling on the main Himalayan
919 thrust. Geophysical Research Letters, 42(14), 5828-5837.

920 Stübner, K., Grujic, D., Dunkl, I., Thiede, R., & Eugster, P. (2018). Pliocene episodic
921 exhumation and the significance of the Munsiari thrust in the northwestern Himalaya. *Earth and*
922 *Planetary Science Letters*, *481*, 273-283.

923 Thakur, V. C. (Ed.). (1992). Geology of western Himalaya (Vol. 19). Pergamon Press.

924 Thakur, V. C., Joshi, M., Sahoo, D., Suresh, N., Jayangondapermal, R., & Singh, A. (2014).
925 Partitioning of convergence in Northwest Sub-Himalaya: estimation of late Quaternary uplift and
926 convergence rates across the Kangra reentrant, North India. International Journal of Earth
927 Sciences, 103(4), 1037-1056.

928 Thiede, R., Robert, X., Stübner, K., Dey, S., &Faruhn, J. (2017). Sustained out-of-sequence
929 shortening along a tectonically active segment of the Main Boundary thrust: The Dhauladhar
930 Range in the northwestern Himalaya. Lithosphere, 9(5), 715-725.

931 Thiede, R. C., Bookhagen, B., Arrowsmith, J. R., Sobel, E. R., & Strecker, M. R. (2004).
932 Climatic control on rapid exhumation along the southern Himalayan Front. Earth and Planetary
933 Science Letters, 222(3-4), 791–806. https://doi.org/10.1016/j.epsl.2004.03.015

934 Turowski, J. M., Lague, D., and Hovius, N. (2009). Response of bedrock channel width to
935 tectonic forcing: Insights from a numerical model, theoretical considerations, and comparison
936 with field data. *Journal of Geophysical Research: Earth Surface*, *114*(F3).

937 Vassallo, R., Mugnier, J. L., Vignon, V., Malik, M. A., Jayangondaperumal, R., Srivastava, P.,
938 and Carcaillet, J. (2015). Distribution of the late-Quaternary deformation in northwestern
939 Himalaya. Earth and Planetary Science Letters, 411, 241-252.

940 Wadia, D. N. (1934). The Cambrian-Trias sequence of north-western Kashmir (parts of
941 Muzaffarabad and Baramula districts). Records of the Geological Survey of India, 68(2), 121-
942 176.

943 Webb, A. A. G., Yin, A., Harrison, T. M., Célérier, J., Gehrels, G. E., Manning, C. E., & Grove,
944 M. (2011). Cenozoic tectonic history of the Himachal Himalaya (northwestern India) and its
945 constraints on the formation mechanism of the Himalayan orogen. *Geosphere*, *7*(4), 1013-1061.

946 Wesnousky, S. G., Kumar, S., Mohindra, R., & Thakur, V. C. (1999). Uplift and convergence
947 along the Himalayan Frontal Thrust of India. Tectonics, 18(6), 967-976.

948 Whipple, K. X., & Tucker, G. E. (1999). Dynamics of the stream-power river incision model:
949 Implications for height limits of mountain ranges, landscape response timescales, and research
950 needs. Journal of Geophysical Research: Solid Earth, 104(B8), 17661-17674.

951 Whipple, K. X., DiBiase, R. A., & Crosby, B. T. (2013). Bedrock rivers. In Treatise on
952 geomorphology. Elsevier Inc..

953 Wobus, C. W., Hodges, K. V., & Whipple, K. X. (2003). Has focused denudation sustained
954 active thrusting at the Himalayan topographic front?. *Geology*, *31*(10), 861-864.

Wobus, C., Heimsath, A., Whipple, K., & Hodges, K. (2005). Active out-of-sequence thrust faulting in the central Nepalese Himalaya. Nature, 434(7036), 1008.

Wobus, C., Whipple, K. X., Kirby, E., Snyder, N., Johnson, J., Spyropolou, K., Crosby, B., Sheehan, D & Willett, S. D. (2006). Tectonics from topography: Procedures, promise, and pitfalls. Special papers-geological society of America, 398, 55.

Yadav, R. K., Gahalaut, V. K., Bansal, A. K., Sati, S., Catherine, J., Gautam, P., Kumar, K., and Rana, N., 2019, Strong seismic coupling underneath Garhwal–Kumaun region, NW Himalaya, India: Earth and Planetary Science Letters, v. 506, p. 8-14.

Yin, A., & Harrison, T. M. (2000). Geologic evolution of the Himalayan-Tibetan orogen. Annual Review of Earth and Planetary Sciences, 28(1), 211-280.

Figure captions

Figure 1: (a) An overview geological map of the western sector of the Indian Himalaya showing major lithology (simplified after Steck, 2003 and Gavillot et al., 2018) and existing structures (Vassalo et al., 2015; Gavillot et al., 2018). The tectonic Kishtwar Window (KW) is surrounded by exposure of the MCT, locally known as the Kishtwar Thrust (KT), and exposes the Lesser Himalayan nappes. The Lesser Himalaya forms a west-verging asymmetric anticline. Apatite fission-track (AFT) ages are adapted from Kumar et al. (1995). (b) A balanced cross-section of the NW Himalaya showing the general architecture of the Himalayan orogenic wedge (simplified from Gavillot et al., 2018). Note that, beneath the KW, Gavillot et al. (2018) proposed the

existence of at least two crustal ramps (MCR-1 and MCR-2) on the MHT, translation on which may have resulted in 3.2-3.6 mm/yr Quaternary exhumation rates across the KW.

Figure 2: Lithological units and structural orientations observed in the Chenab valley. (a) Steeply-dipping HHCS units near the western margin of the KW. (b) Highly-deformed migmatites at the base of the KT. (c) Sub-vertical quartzite slabs of Chail Formation exposed in the frontal horses of the LH Duplex (or, anticline). (d) Highly-deformed, sub-vertical and pervasively folded and compressed quartzite layers within the core of the KW, the base of stacked LH-nappes forming the hanging wall of the proposed surface-breaking fault (Fig. 8d). (e) A close-up view of the folded quartzite units. (f) Steeply-dipping units of granite which formed new penetrative foliation outcropping upstream from the fault-zone. (g) Further upstream from the fault-zone, the bedrocks are gentler in the eastern edge of the KW.

Figure 3: Geomorphic features observed along the Chenab River across the KW. (a) Where the Chenab River enters the KW, the major tributaries coming from the Zansar Range in the north are characterized by 'U-shaped' valley suggesting repeated glacial occupancy during the Quaternary. The Chenab valley is unusually wide here providing space for transient storage of glacial outwash sediments. The present-day River re-incises these sedimentary fills. Photograph was taken near the town of Padder (cf. Fig.1a). (b) At the core of the KW, the Chenab valley is V-shaped. The Chenab River is steep and maintains a narrow channel width. (c) Highly-elevated fluvial strath surfaces are preserved in the vicinity of the town of Kishtwar Fluvial incision observed along the N-S traverse of the Chenab River. Photograph was taken from south of the Kishtwar town. The Kishtwar surface (~400m high from the river) is underlain by ~150-170m thick sediment cover overlying the tilted Higher Himalayan bedrock. The River has incised another ~240m bedrock in this section. (d) Epigenetic gorge formed along the Chenab River in

its' N-S traverse through the HHCS. The town of Drabshalla is built on the hillslope deposits. (e) Chenab River maintained very narrow channel (width: ~20-25 m) through moderately-strong HHCS rocks, suggesting tectonic imprint on topography. (f) Formation of knickpoint at the confluence of the tributary with the trunk stream implying rapid fluvial incision of the trunk stream. (g) Three levels of strath surfaces observed below the Kishtwar surface. The strath levels are marked as T1 (~280m), T2 (~170m) and T3 (~120m). OSL dating of fluvial sediments lying above the T3 surface yield a minimum depositional age of ~21.6±2.6 ky.

Figure 4: (a) Lithological distribution near the western margin of the KW (cf. Fig.8 for location). Luminescence sample (OSL and IRSL) locations and respective depositional ages (in kyr) are shown. Every sample except K16 and K17 were taken above strath level T1. K16 and K17 were taken from above the T3 level. Note that, the ages reported in italics are minimum age estimates. (b) A field photograph from the village Janwas, south of the town of Kishtwar, showing the aggraded sediments lying above the Higher Himalayan tilted bedrock units. (c) IRSL ages (in kyr) from the fluvioglacial sediments and OSL age (in kyr) from the hillslope debris units suggest the valley aggradation probably started at the transition of the glacial to interglacial phase ~120-130 kyr and continued till ~80 kyr ago. (d) A close-up view (red rectangle in fig.4c) of the tilted fluvioglacial sediment layers showing alternate conglomerate and medium-coarse sand layers. (e) A ~3m thick fine sand layer within the hillslope debris yield depositional age of ~86±5 kyr. Photograph was taken near the village Pochal, northwest of the town of Kishtwar.

Figure 5: Regional variations in (a) topography, (b) topographic relief (moving window of ~4 km) (c) TRMM-derived rainfall (after Bookhagen and Burbank, 2006), and (d) basinwide normalized steepness indices (ksn value) of the region shown dashed box in Figure 1a. 12.5 m

ALOS PALSAR DEM, downloaded from https://asf.alaska.edu/ was used as the topography data (e) Swath profiles (swath window: 50 km) along the line AB (cf. Fig.5a) demonstrate the orogen-perpendicular variations in elevation, rainfall and ksn value. KW is characterized by high elevation, high relief and high steepness, but low rainfall.

Figure 6: Longitudinal profile of the Chenab River shows major changes in channel gradient associated with knickpoints in the upstream. It illustrates that the major changes in the channel gradient extend over the full length of the KW and strongest changes are located in the core and not at the margins of the window. We classified knickpoints on the basis of their genesis. The substrate lithology along the River is shown. Knickpoints caused by glacial occupancy (G1, G2 and G3) are adapted from Eugster et al. (2016), who reconstructed the timing of maximum glaciation and extent of glacial cover in source region of upper Chenab River basin during the last glacial maximum. These knickpoints highlight the importance of glacial erosion in the high-elevation sectors, especially in the northern tributaries of the Chenab River. Further in this study, we focused on the area marked by red rectangle.

Figure 7: Along-river variations in (a) channel-elevation, (b) channel width, (c) channel gradient, (d) normalized steepness index, and (e) rock-strength of non-fractured bedrock units (R-value taken by rebound hammer) till 165 km upstream from the MBT (point X, cf. Fig.1a). The mean R-value$\pm\sigma$ for each rock type has been plotted against their spatial extent. We identified two distinct zones (K1 and K2) of high channel gradient and steepness index, which maintain low channel width despite the variable rock strength of the substrate. Knickpoint KP4 may have been generated by the formation of the epigenetic gorge along the N-S traverse of the Chenab River (cf. Fig.3c). Knickpoints KP1 and KP5 mark the transition of a soft-to-hard bedrock substrate.

Figure 8: (a) Detailed structural data from the study area showing structural and lithological variations (modified after Steck, 2003; Gavillot et al., 2018). (b) and (c) Orogen-perpendicular drop of the Chenab trunk stream across stretch 1 and stretch 2, respectively, showing transient increase in steepness over the K1 and K2 knickzone. The orthogonal profile projection method has been used in the case of K2 (cf. fig.7) to identify the width of the steep segment. (d) Comparison between two deformation models explaining the observed morphometric variations across the KW – (a) duplex-growth model (adapted from Gavillot et al., 2018) and (b) active out-of-sequence fault model.

Figure 9: A satellite image of the northern Kishtwar town showing the present-day flow-path of the Chenab River (cf. Fig.8 for location). Hillslope debris originated from the steep western margin of the KW (only made of massive white quartzites) and was deposited over fluvioglacial and glacio-lacustrine sediments and Higher Himalaya schists bedrock exposed below in the Kishtwar valley. Massive hillslope sediment flux impeded the paleo-drainage system leaving behind the paleo-valley of the tributary, the Maru River. Our interpretation of the paleo-drainage is marked in a white dashed line. (a) A view of the Kishtwar surface from the western margin of the KW showing present-day gorge of the Chenab River and its tributary. The wind-gap (paleo-valley) of the tributary is visible. (b) Thick clay-silt deposit in the wind-gap suggests abandonment of river-flow. The OSL sample is saturated and hence only denotes the minimum age of valley abandonment/ hillslope debris flow. (c) Overview picture of the frontal horses of the LH duplex and the direction of debris flow towards the Kishtwar town. (d) Angular, poorly-sorted clasts and boulders were observed at the base of the debris flow unit near the village of Pochal, north of the Kishtwar town. The white quartzites of LH are exposed in the vicinity of the

Kishtwar Town (see satellite image) – only the eastern valley flank can have collapsed in the past.

Figure 10: (a) A topographic and geomorphic profile across the Chenab valley drawn over the Kishtwar Town. The valley aggradation by fluvioglacial and hillslope debris sediments was succeeded by a fluvial incision which penetrated through the unconsolidated sediments of thickness ~140-150m and incised Higher Himalayan bedrock by ~280±5 m, leaving behind at least three recognizable strath surfaces with a thin late Pleistocene sediment cover. The three strath surfaces are at 280±5 m (T1), ~170 m (T2), and ~120±5 m (T3) heights from the present-day River. We assume that the present-day bedrock gorge has been carved since the deposition of the glacio-lacustrine sediment deposits (~100-130 ky) and the hillslope debris (~90-80 ky) onto former fluvial strath surface of Higher Himalayan Bedrock. The width of the fluvial strath surface where the Kishtwar Town is located indicates that the river network had been dammed earlier too. (b) Graphical representation of mean bedrock incision rates since 80 kyr. Age constraints for T3 are shown in Fig. 4a. Based on relative heights and depositional ages of late Pleistocene deposits, we propose a minimum and a maximum bedrock incision rate of 3.1-3.5 mm/y and 5.2-5.6 mm/yr, respectively. In contrast, further downstream, the bedrock incision rates calculated from bedrock straths farther downstream from the KW range 0.7-0.8 mm/yr.

Table caption:

Table 1: Calculations of change in specific stream power (SSP) values across the ramp and the flat segments beneath the LH Duplex. We used a uniform discharge for SSP calculation.

Table 2: Sample locations, elemental concentrations, dose rates, equivalent doses and age estimations for OSL and IRSL analyses of sand samples from Kishtwar valley.

Figures

Figure 1

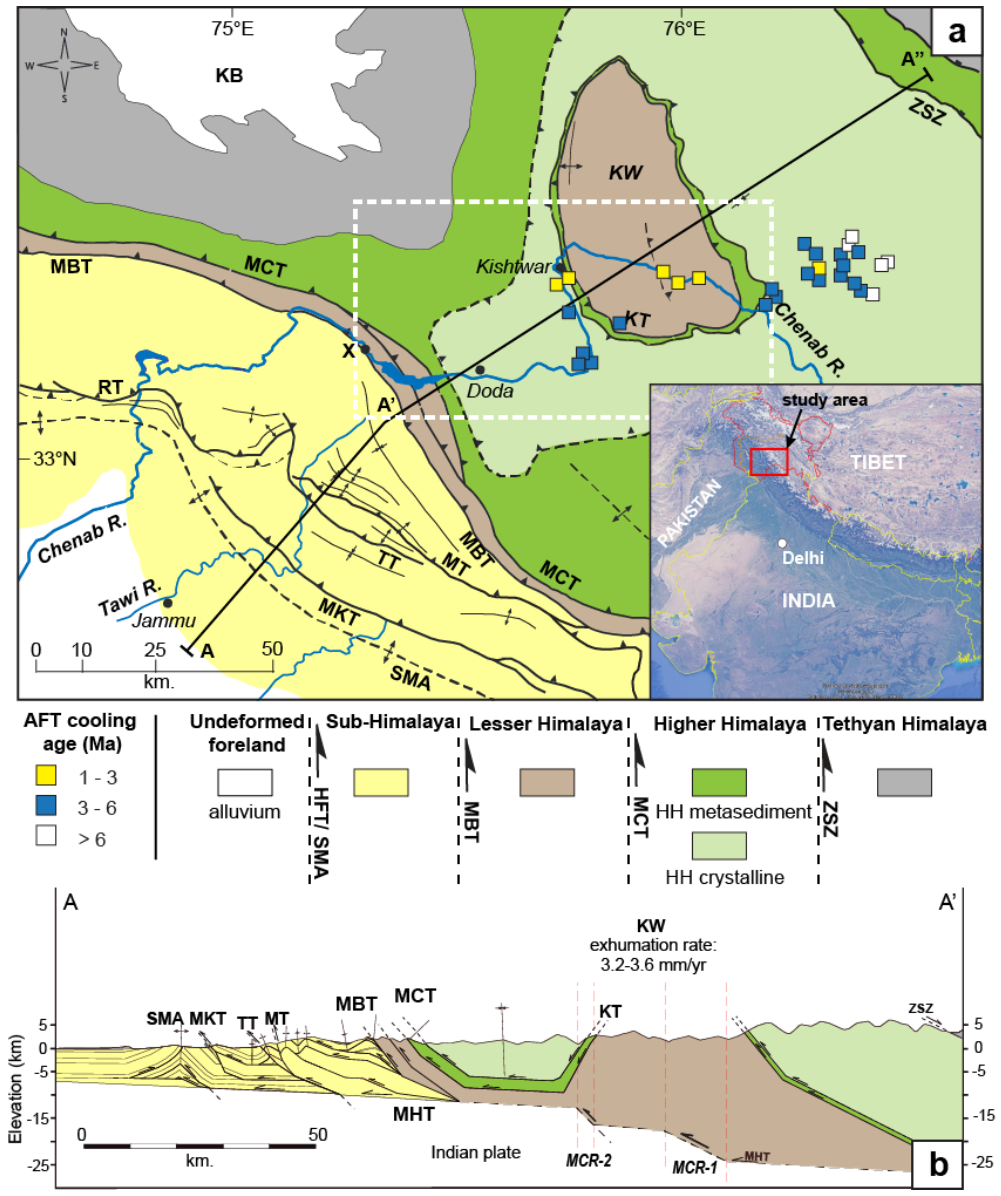

1095 Figure 2

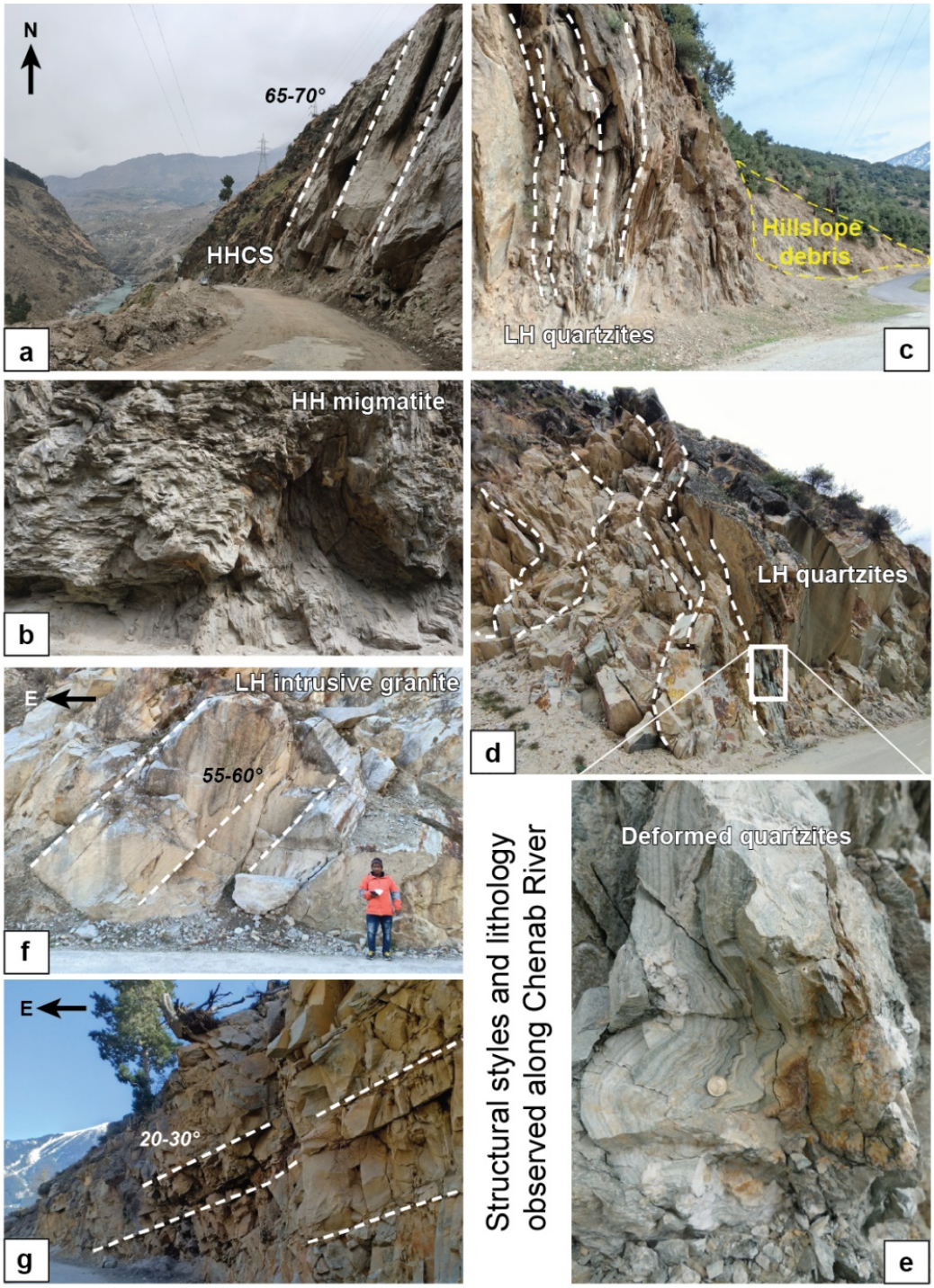

Structural styles and lithology observed along Chenab River

1096

1097

1098 Figure 3

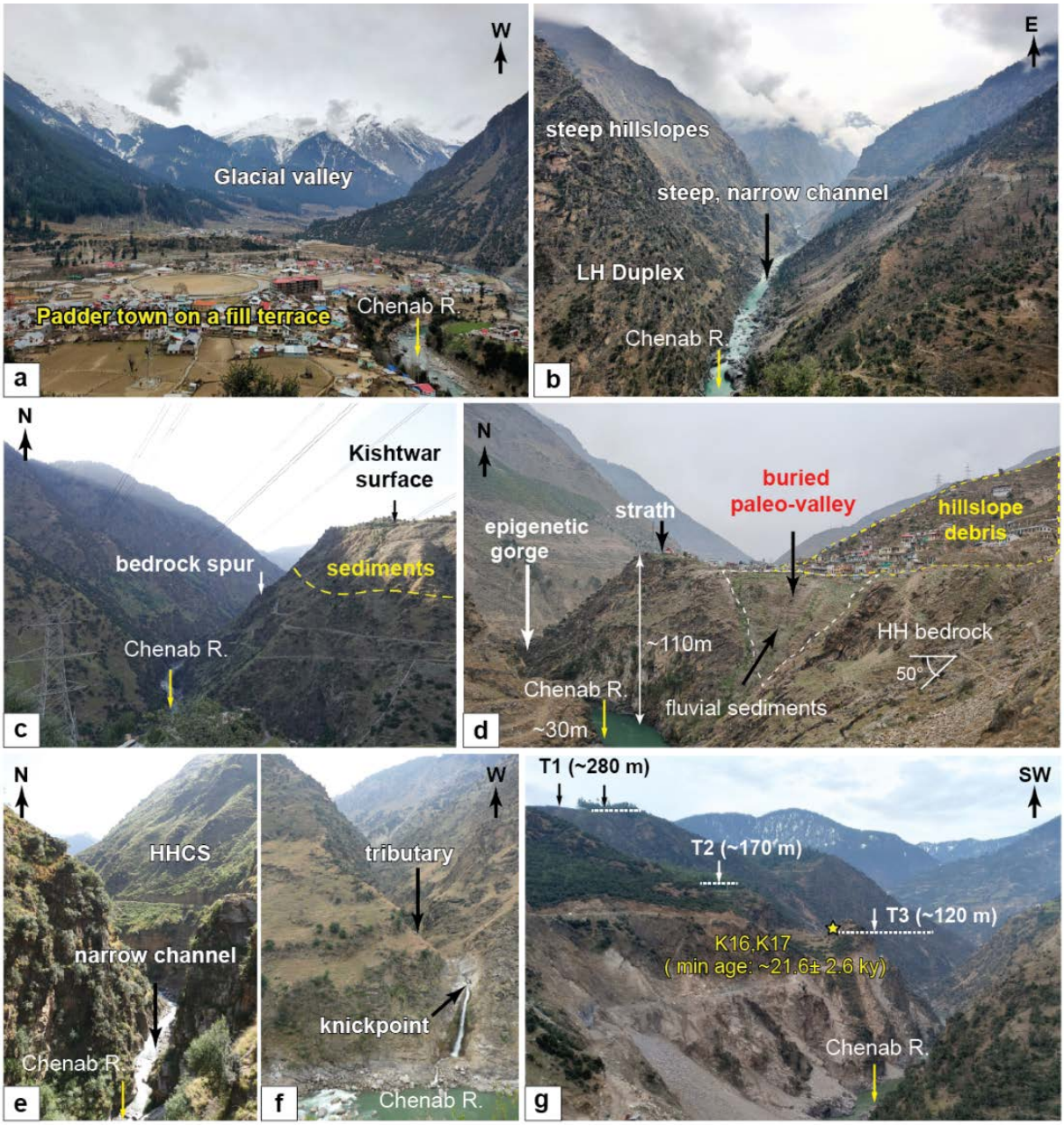

1099

1100

1101 Figure 4

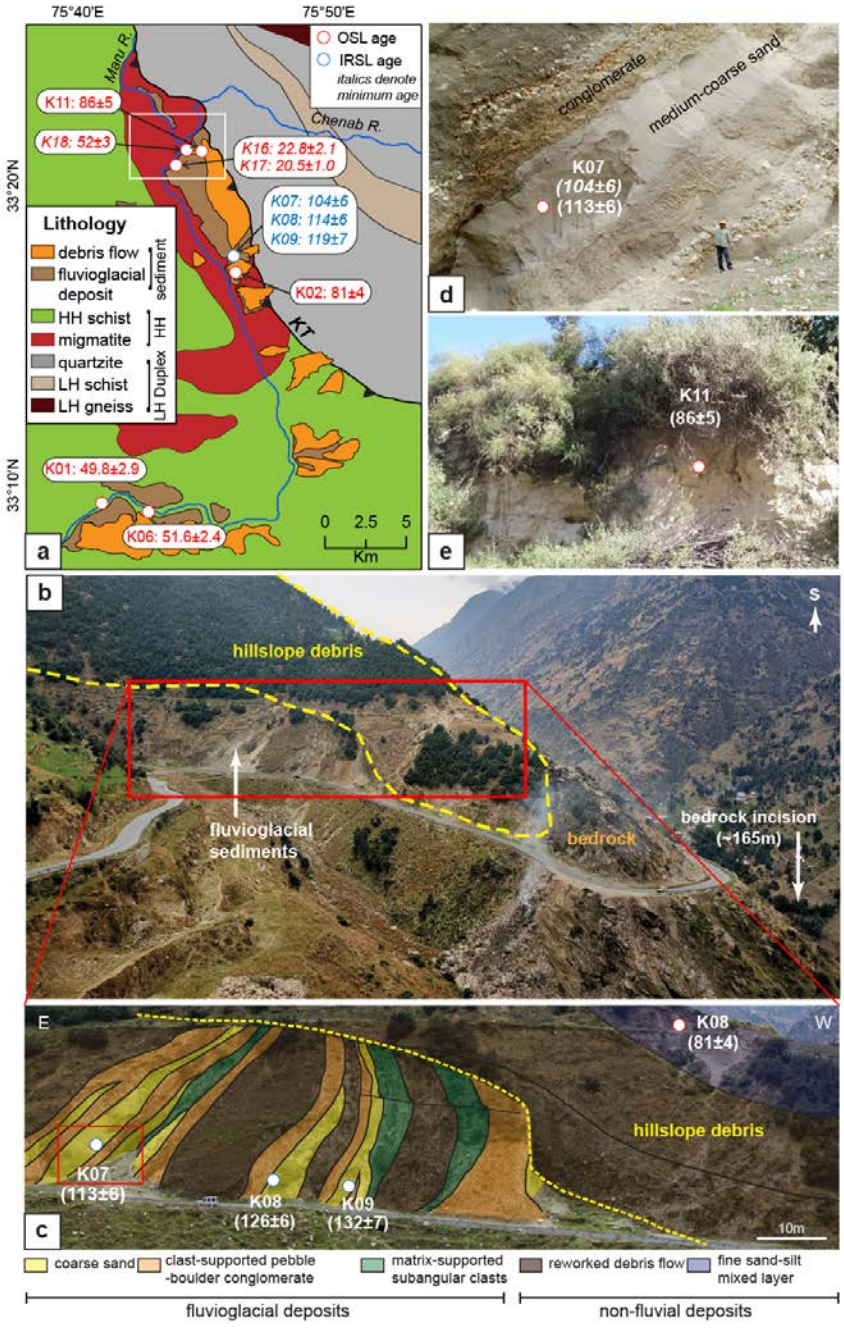

1102

1103

1104 Figure 5

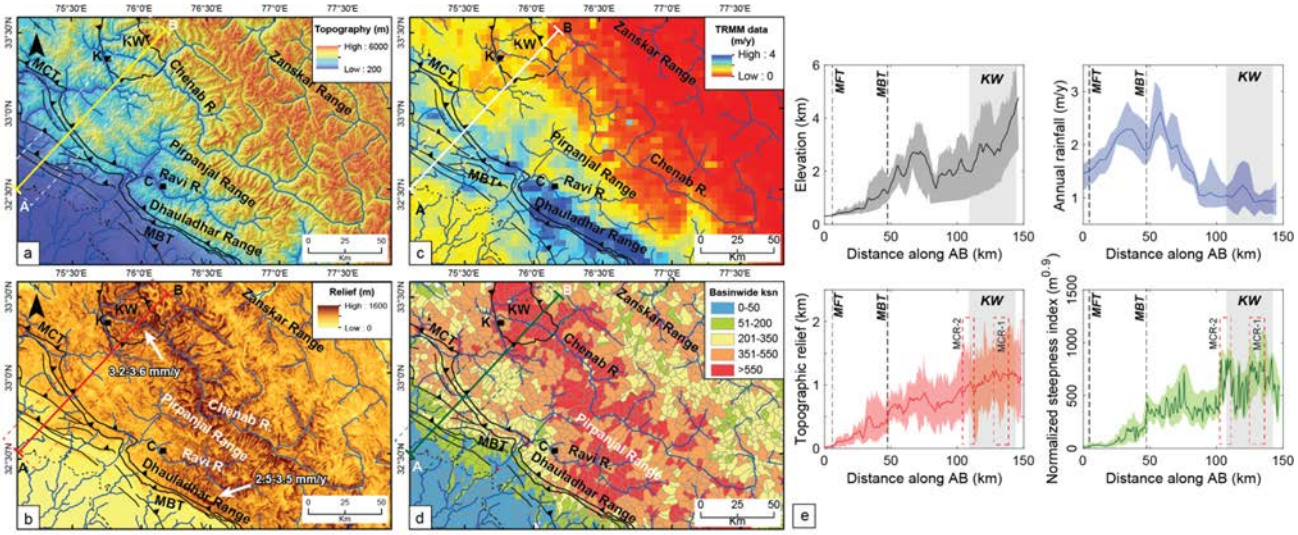

1105

1106

Figure 6

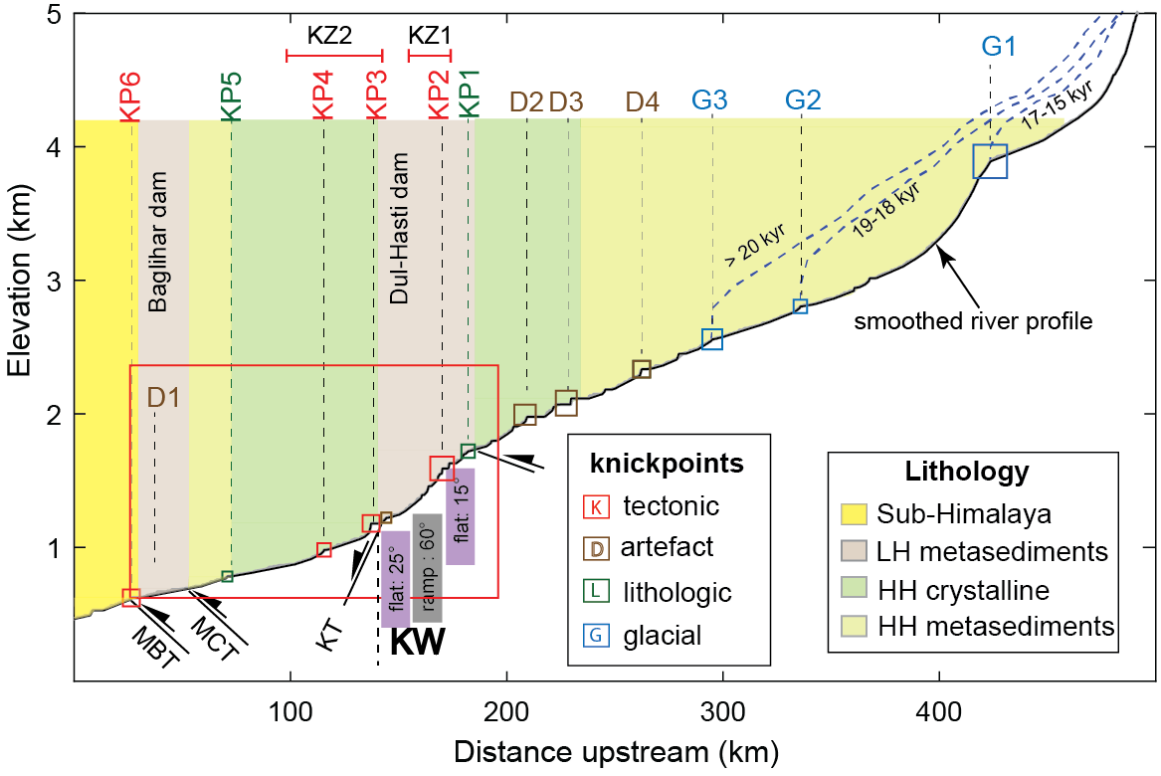
KZ2
KZ1
KP6
KP5
KP4
KP3
KP2
KP1
D2 D3
D4
G3
G2
G1
17-15 kyr
19-18 kyr
> 20 kyr
Baglihar dam
Dul-Hasti dam
D1
smoothed river profile
flat: 25°
ramp : 60°
flat: 15°
MBT
MCT
KT
KW
knickpoints
K tectonic
D artefact
L lithologic
G glacial
Lithology
Sub-Himalaya
LH metasediments
HH crystalline
HH metasediments
Elevation (km)
Distance upstream (km)
1
2
3
4
5
100
200
300
400

1110

Figure 7

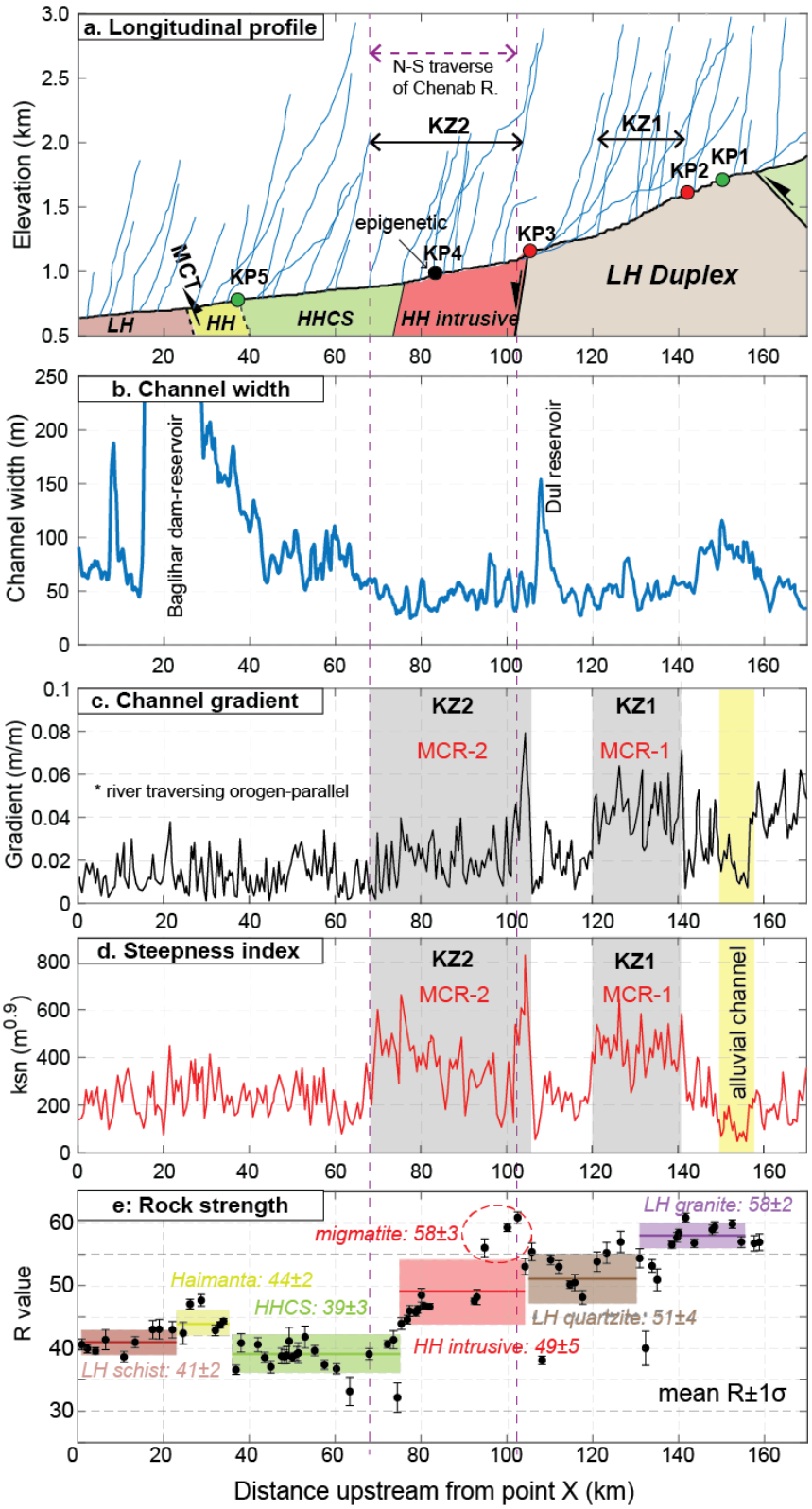

1111

1112

Figure 8

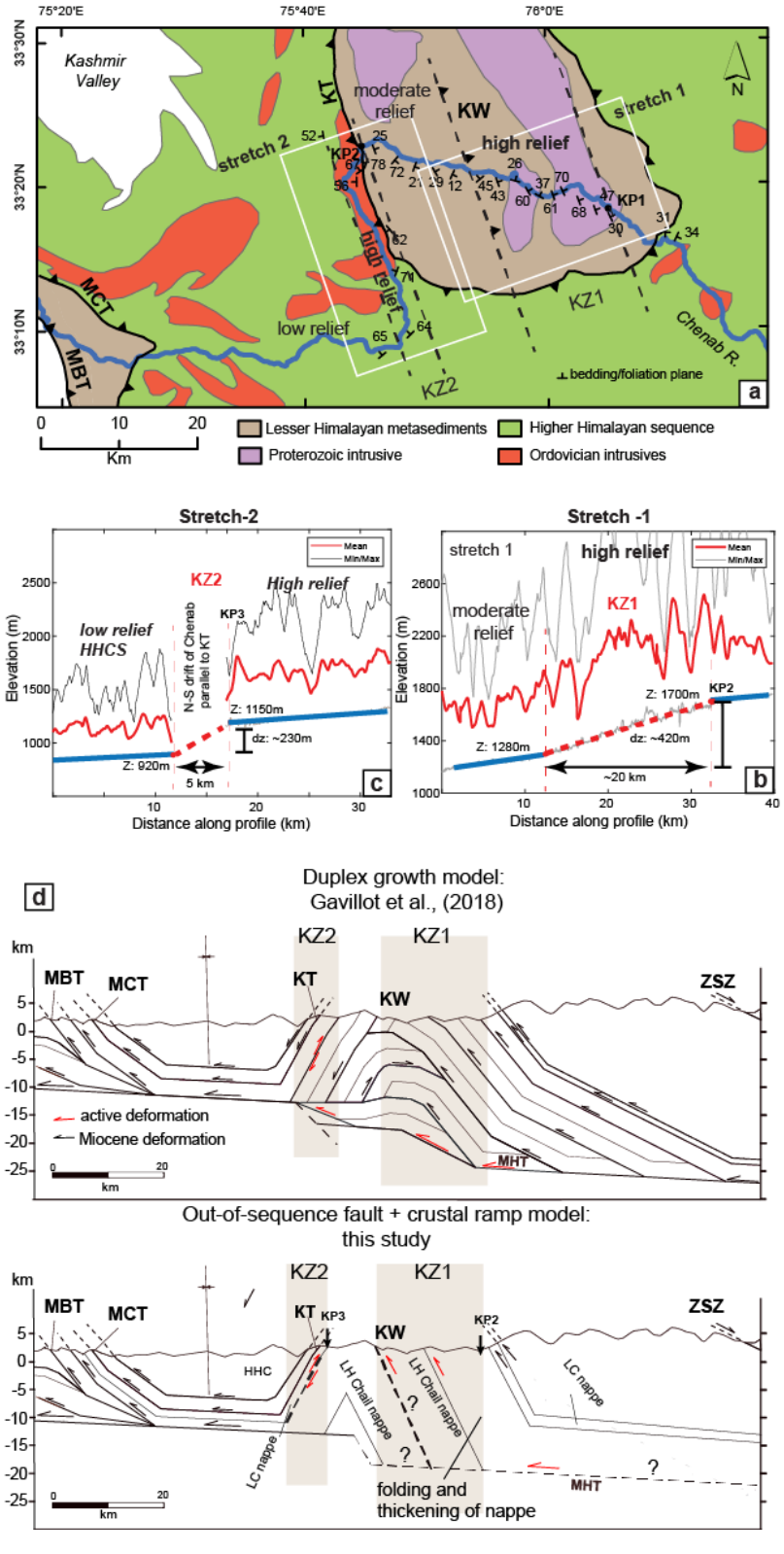
75°20'E
75°40'E
76°0'E
33°30'N
33°20'N
33°10'N
Kashmir Valley
KT
moderate relief
KW
stretch 1
stretch 2
high relief
KP2
KP1
high relief
MCT
low relief
KZ1
Chenab R.
MBT
KZ2
bedding/foliation plane
a
0 10 20
Km
Lesser Himalayan metasediments
Higher Himalayan sequence
Proterozoic intrusive
Ordovician intrusives
Stretch-2
KZ2
High relief
low relief
HHCS
KP3
N-S drift of Chenab parallel to KT
Z: 1150m
dz: ~230m
Z: 920m
5 km
Elevation (m)
Distance along profile (km)
c
Stretch -1
stretch 1
high relief
moderate relief
KZ1
Z: 1700m
KP2
Z: 1280m
dz: ~420m
~20 km
b
d
Duplex growth model:
Gavillot et al., (2018)
km
MBT
MCT
KT
KZ2
KZ1
KW
ZSZ
active deformation
Miocene deformation
MHT
Out-of-sequence fault + crustal ramp model:
this study
HHC
LC nappe
LH Chail nappe
folding and
thickening of nappe

Figure 9

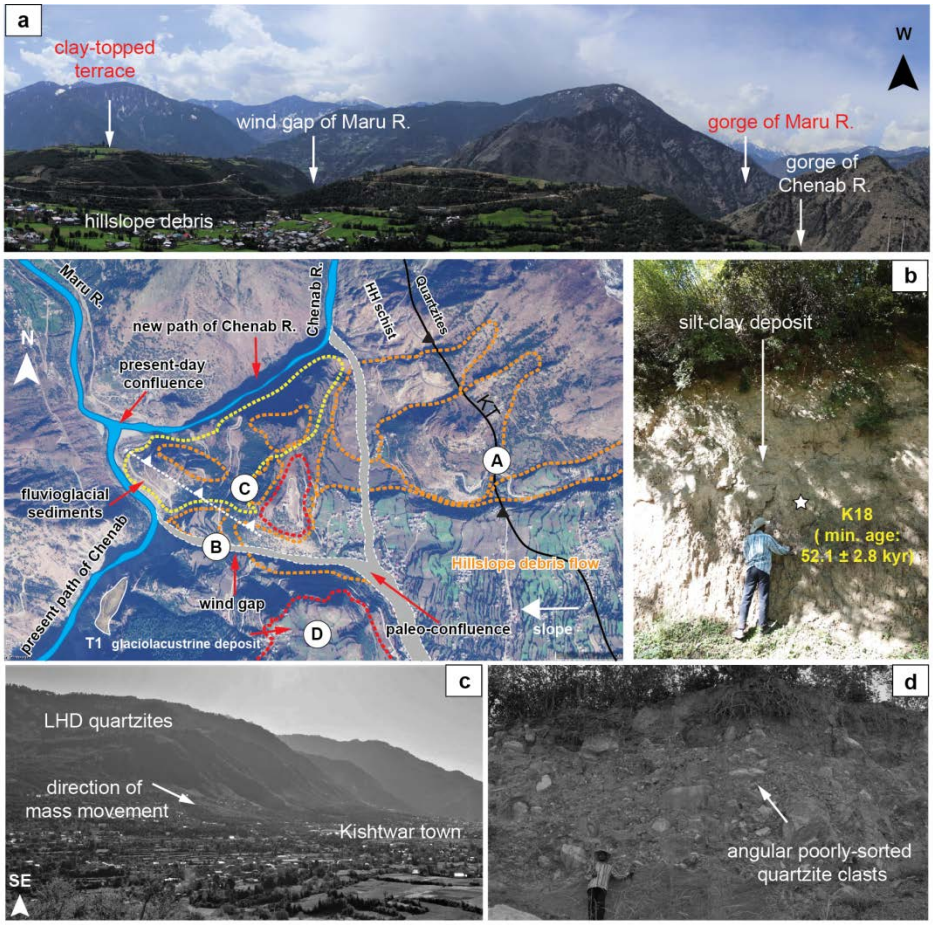
a
clay-topped terrace
wind gap of Maru R.
gorge of Maru R.
gorge of Chenab R.
hillslope debris
W
Maru R.
Chenab R.
HH schist
Quartzites
KT
N
new path of Chenab R.
present-day confluence
fluvioglacial sediments
present path of Chenab
T1
glaciolacustrine deposit
wind gap
paleo-confluence
Hillslope debris flow
slope
A
B
C
D
b
silt-clay deposit
K18
(min. age:
52.1 ± 2.8 kyr)
c
LHD quartzites
direction of mass movement
Kishtwar town
SE
d
angular poorly-sorted quartzite clasts

1119 Figure 10

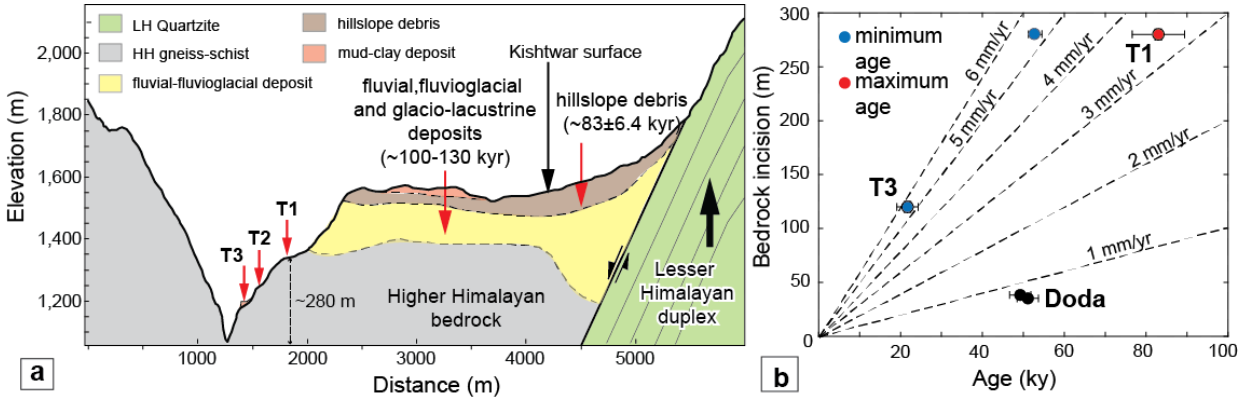

1120

1121

1122 Table 1

1123

Parameter	downstream	KZ1	% change	ratio KZ1:downstream	downstream	KZ2	% change	ratio KZ2:downstream
average channel gradient (m/m)	0.006	0.021	250	3.5	0.01	0.046	360	4.6
average channel width (m)	70	45	-35.71	0.6	55	42	-24	0.76
*Specific stream power (SSP)	0.000086	0.000467	444.44	5.4	0.000182	0.001095	502	6.02

* SSP calculated by assuming equal-discharge (Q)

1124

Table 2

Sample type	Sample name	Lat (°)	Long (°)	U (ppm)	Th (ppm)	K (%)	water (%)	Dose rate (Gy/ky)	De (Gy)	OD (%)	Age (ky)	fading correction	Corrected age (ky)
using central age model													
OSL	K02	33.29607	75.77619	3.8	7.2	0.46	6.1	1.74±0.02	141±8	19.5	81.1±4.6		
OSL	K11	33.35352	75.74649	3.1	12.7	2.41	6	3.97±0.09	341±19	16.8	85.7±5.1		
OSL	K01	33.15222	75.66323	2.9	13.2	2.03	9	3.88±0.04	193±11	22.1	49.8±2.9		
OSL	K06	33.15243	75.70609	3.4	18	2.17	5.4	3.97±0.05	205±10	14.4	51.6±2.4		
IRSL	K07	33.2778	75.76922	3.3	13.8	2.31	5.3	4.67±0.22	489±29	16.8	104.5±5.9	0.89	113±6
IRSL	K08	33.2778	75.76922	3.5	16.9	1.97	5.6	4.61±0.23	528±38	20.5	114.4±6.3		
IRSL	K09	33.2778	75.76922	3.3	12.2	1.98	4.8	4.29±0.20	510±42	18.1	119.2±6.8	1.11	132±7
using minimum age model													
OSL	K16	33.34873	75.73324	3.5	16.8	2.03	7.5	3.95±0.1	90±8	40	22.8±2.1		
OSL	K17	33.34873	75.73324	3.4	18	2.17	10.5	3.96±0.11	81±3.5	46	20.5±1.0		
saturated sample													
OSL	K18	33.35176	75.74325	3.3	18.7	2.61	4.5	4.36±0.13	227±14		52.1±2.8		